ORIGINAL PAPER

M. Scambelluri · J. Hermann · L. Morten
E. Rampone

Melt- versus fluid-induced metasomatism in spinel to garnet wedge peridotites (Ulten Zone, Eastern Italian Alps): clues from trace element and Li abundances

Abstract The peridotite bodies of the Ulten Zone (Upper Austroalpine, Italian Eastern Alps) are enclosed in Variscan migmatites and derive from a mantle wedge environment. They display the progressive transformation of porphyroclastic spinel peridotites ($T = 1{,}200°C$; $P = 1.5$ GPa) into fine-grained garnet–amphibole peridotites ($T = 850°C$; $P = 3$ GPa). Detailed bulk-rock and mineral trace element analyses of a sample suite documenting the entire metamorphic evolution of the peridotites revealed several stages of metasomatism. The spinel peridotites derive from a depleted mantle that became enriched in some large ion lithophile element (LILE) and light rare earth elements (LREE). The same signature pertains to clinopyroxene and orthopyroxene, indicating that this metasomatic signature was acquired at the recorded temperature of 1,200°C. Such a temperature is considerably above the wet peridotite solidus and hence the metasomatic agent must have been a hydrous melt. Moreover, the Li-enrichment of the spinel-facies pyroxenes (up to 24 ppm Li) reflects disequilibrium distribution after exchange with a presumably mafic melt. $^{cpx/opx}D_{Li} = 3$–7 and $^{cpx/ol}D_{Li} = 2.7$–8 indicate that the spinel-facies clinopyroxene hosts higher Li amounts than the coexisting minerals. LREE fractionation, variable LREE enrichment, LILE enrichment with respect to HFSE (average clinopyroxene $Pb_N/Nb_N = 16$–90) in spinel lherzolites can be related to chromatographic effects of porous melt flow. The significant enrichment of pyroxenes from the spinel lherzolites in Pb, U and Li indicates that the metasomatic melt was subduction-related. All these features suggest that the spinel lherzolites formed a mantle wedge layer percolated by melts carrying recycled crustal components and rising from a deeper source of subduction magmas. The garnet + amphibole peridotites equilibrated at temperatures well below the wet solidus in the presence of an aqueous fluid. Bulk-rock trace element patterns display pronounced positive anomalies in Cs, Ba, Pb and U and moderate enrichment in Li, indicating addition of a crustal component to the mantle rocks. Amphibole hosts most of these trace elements. Clinopyroxene displays high LILE/HFSE ($Pb_N/Nb_N = 300$–600), low Ce/Pb (1.4–2.7 in garnet-facies clinopyroxene compared with 2.6–24.5 in the spinel-facies one) and variable LILE and LREE enrichments. The coupled increase of modal amphibole, Sr and Pb, together with positive Pb–Sr and Pb–U correlations, further indicate that incompatible element influx in these samples was fluid-mediated. In the garnet-facies samples, amphibole and, interestingly, olivine have similarly high Li concentrations as clinopyroxene, leading to $^{cpx/amph}D_{Li} = 0.7$ and $^{cpx/ol}D_{Li} = 0.7$–0.8, the latter being up to ten times lower than in the spinel-facies rocks. Due to its high modal abundance, olivine is the main host of Li in the garnet–amphibole peridotites. The observed metasomatic features provide evidence for the infiltration of an aqueous fluid in the mantle wedge above a subducting slab. This fluid most likely derived from subducted crustal rocks that underwent partial melting. Successive retrograde re-equilibration during exhumation of the garnet peridotite is accompanied by garnet and clinopyroxene breakdown and amphibole formation.

M. Scambelluri (✉) · E. Rampone
Dipartimento per lo Studio del Territorio e delle sue Risorse,
University of Genova, Corso Europa 26, 16132 Genova, Italy
E-mail: marco.scambelluri@dipteris.unige.it
Tel.: +39-010-5358315
Fax: +39-010-352169

J. Hermann
Research School of Earth Sciences, The Australian National
University, 0200 Canberra, ACT, Australia

L. Morten
Dipartimento di Scienze della Terra e Geologico Ambientali,
Università di Bologna, Piazza di Porta S. Donato 1,
40126 Bologna, Italy

This process produced minor changes, such as an increase of HREE and Li in amphibole, and an increase of Li in olivine. The general trace element signature remains essentially unchanged during retrogression and further hydration, indicating that fluids with a similar composition to the one present at the garnet–amphibole peridotite formation, were responsible for increased amphibole formation. The combined evidence from the metamorphic and metasomatic evolution indicates that the peridotites experienced first corner flow in a mantle wedge, followed by subduction and finally entrapment and exhumation within a crustal slab. During their entire history the Ulten peridotites were percolated first by melts and then by aqueous fluids, which added recycled crustal components to the mantle wedge.

Introduction

Subduction zones are the Earth's environments where the consumption of oceanic and continental lithosphere and the creation of new continental crust occur in a continuous cycle. In this scenario, the fluid phase released by the dehydration of the subducting plate is a viable agent for slab-to-mantle element transfer, mantle metasomatism and melting. The composition of the metasomatized mantle and the dynamics of the mantle wedge ultimately control magma production at subduction settings (Tatsumi 1989; van Keken 2003). Most subduction-zone magmas are generated in a metasomatized mantle source with the exception of adakitic magmas, which are attributed either to melting of the slab, or of a mantle domain contaminated by slab-derived liquids (Martin et al. 2005). A general consensus exists that the fluid phase released during subduction is enriched in several incompatible elements (i.e. large ion lithophile, light and rare earth elements). In detail, however, the mechanisms of element partitioning among fluid/melt and mineral phases at variable pressure, temperature and fluid composition are highly debated (Brenan et al. 1995; Scambelluri and Philippot 2001; Manning 2004; Kessel et al. 2005). There is emerging evidence that the light elements Be, Li and B are particularly sensitive tracers of the slab-to-mantle transfer of fluids (Domanik et al. 1993; Bebout and Barton 1993; Moran et al. 1992; Leeman 1996; Brenan et al. 1998; Woodland et al. 2002; Zack et al. 2003; Scambelluri et al. 2004; Elliott et al. 2004; Tenthorey and Hermann 2004). Li, in particular was recently used as monitor of metasomatism in mantle rocks which interacted either with melts (Seitz and Woodland 2000), or with solute-rich, aqueous fluids (Paquin and Altherr 2002; Paquin et al. 2004).

Although geochemical and petrologic research has recently focussed on fluid/melt/rock interactions in subduction zone environments, still few are the direct studies of rocks from the mantle wedge, which remains the least known domain within the subduction factory. The main source of information derives from mantle xenoliths of supra-subduction settings, containing amphibole, phlogopite as main metasomatic minerals (Vidal et al. 1989; Maury et al. 1992; Szabo et al. 1996; Laurora et al. 2001) and locally trapping aqueous fluid inclusions, or silicate glass inclusions with amphibole and phlogopite daughter minerals (Trial et al. 1984; Schiano et al. 1995; Andersen and Neumann 2001). Most of these xenoliths formed at pressures corresponding to the fore-arc region: the interactions between subduction fluids/melts and wedge peridotites at sub-arc depths are therefore still poorly constrained. Relevant information can be gained from particular orogenic garnet peridotites, which are attributed to slices of a mantle wedge that is tectonically engaged inside subducted continental slabs (Brueckner 1998; Nimis and Morten 2000; Van Roermund et al. 2002). These rocks preserve the mineralogical and geochemical records of metasomatic processes that affected mantle domains percolated by aqueous fluid and hydrous melt sourced from crustal slab reservoirs (Rampone and Morten 2001; Paquin et al. 2004; Zheng et al. 2005).

We investigate the interaction of melts and aqueous fluids with mantle wedge peridotites using bulk-rock and mineral trace element data on a peridotite sample set from the Ulten Zone (Tonale Nappe, Upper Austroalpine Domain, Italian Eastern Alps). These peridotites form bodies inside migmatized continental rocks, and display progressive transformation of spinel lherzolites to garnet–amphibole peridotites (Obata and Morten 1987). This evolution has been interpreted as burial and cooling of spinel peridotites as the result of corner flow in the mantle wedge followed by tectonic entrapment into a subducting continental slab (Godard et al. 1996; Nimis and Morten 2000). Evident metasomatic features in the garnet peridotites are formation of amphibole $\pm$ phlogopite and progressive increase in large ion lithophile element (LILE) and light rare earth element (LREE), suggesting the influx of slab-derived aqueous fluids at relatively low temperature (Morten and Obata 1990; Rampone and Morten 2001). In addition to the fluid-mediated slab/peridotite interaction emphasized by the previous studies, we present petrologic and trace element evidence for an earlier, high-temperature, criptic metasomatism in the spinel-peridotites that we attribute to melt percolation. We show that Li, LILE and LREE in bulk rock and minerals are useful monitors to decipher metasomatic processes in mantle rocks. Our data point to a change from mafic melt to aqueous fluid as the metasomatic agent percolating the mantle wedge peridotites during their pathway towards the slab.

Geologic and petrologic background

The Ulten Zone (Nonsberg), peridotites form lenses of variable size inside gneisses and migmatites of the high-grade Upper Austroalpine basement (Italian Eastern Alps). This basement mostly records the Variscan orogenic cycle, featuring subduction of the continental crust

that presently encloses the garnet peridotite slices. The Alpine orogenesis only marginally affected this composite basement. The high-grade crustal rocks are subdivided in (1) a lower unit, with strongly foliated, weakly migmatized, garnet + kyanite gneisses and (2) an upper unit made of strongly migmatized garnet + kyanite gneiss. Both units include amphibolite lenses which locally preserve peak eclogitic assemblages (Godard et al. 1996). The peridotite bodies are mostly distributed at the transition between the lower and upper gneiss units. The country gneiss and the associated mafic rocks share a common evolution from eclogite-, to granulite-, to amphibolite-facies conditions. Maximum pressures and temperatures recorded by the gneiss and migmatites are estimated at 1.5–2 GPa and 700–850°C (Benciolini and Poli 1993; Hoinkes and Thoeni 1993; Godard et al. 1996; Tumiati et al. 2003). Migmatization at this stage likely occurred under water-absent conditions by phengite dehydration-melting at temperatures of about 850 and minimum pressures of 1.5–2.5 GPa (Benciolini and Poli 1993; Godard et al. 1996; Tumiati et al. 2003). Partial melting in the crustal units at high pressure conditions either occurred during prograde subduction, or during exhumation of deeply buried crustal slices (discussion by Tumiati et al. 2003). The partial melting reactions continued during the exhumation to shallower (granulite-facies) levels thereby obliterating the high-pressure relics in migmatized gneisses (Godard et al. 1996).

The peridotites form metric to decametric lenses with textures changing from coarse porphyroclastic spinel lherzolites, to fine grained amphibole + garnet-bearing lherzolites (Obata and Morten 1987). Pressure–temperature estimates for the spinel-facies assemblage are 1.3–1.6 GPa and 1,200°C (Nimis and Morten 2000). At this stage the spinel peridotites were fluxed by hot hydrous melts rising from deeper regions, crystallizing coarse garnet-free pyroxenite layers in the host peridotites (Nimis and Morten 2000). The coarse spinel in lherzolites is overgrown by coronitic garnet. In the field, the spinel peridotites with coronitic garnet grade into garnet + amphibole peridotite mylonites. These features indicate that the majority of peridotite bodies in the Ulten zone record the transformation of lithospheric spinel lherzolites into garnet + amphibole and amphibole peridotites during a continuous P–T history (Nimis and Morten 2000). The pyroxenite layers record an evolution comparable with the one of the host peridotites and change to fine-grained garnet + amphibole websterites (Morten and Obata 1983; Nimis and Morten 2000). The pressures and temperatures of garnet peridotite formation are evaluated at 850°C and about 2.7 GPa (Fig. 1; after Nimis and Morten 2000). This evolution likely reflects the progressive transition and tectonic emplacement of the hot wedge spinel peridotites into a subducting continental slab, with consequent cooling and pressure increase (Nimis and Morten 2000). This overall process is accompanied by intense deformation and hydration of the peridotite slices to form neoblastic garnet + amphibole-bearing assemblages

(Obata and Morten 1987). Besides amphibole, additional metasomatic minerals in the garnet peridotite are phlogopite, apatite, dolomite and rare Mg-allanite (Obata and Morten 1987; Tumiati et al. 2003). In some peridotites the modal increase of amphibole is accompanied by progressive decrease and disappearance of clinopyroxene and garnet, to produce olivine + amphibole + orthopyroxene + spinel rocks (Obata and Morten 1987). This was interpreted as the result of increasing water activity in the system at still high pressure–temperature conditions, driving to progressive amphibole growth after clinopyroxene and garnet. The metasomatic imprint related with the syn-tectonic hydration of the mantle slices is characterized by significant enrichment in LILE and LREE, to testify the influx of slab-derived fluids (Rampone and Morten 2001).

Sample description

We have chosen a sample suite that is representative of the transformation sequence from spinel-, to garnet + amphibole-, to amphibole-bearing assemblages portrayed in Fig. 1. Most samples record a full textural and chemical equilibration during a single stage of the evolution. All samples are well characterized by previous studies (Obata and Morten 1987; Morten and Obata 1990; Nimis and Morten 2000; Rampone and Morten 2001). Hereafter we present a brief description of the investigated samples, from preserved spinel-lherzolites to amphibole-bearing peridotites.
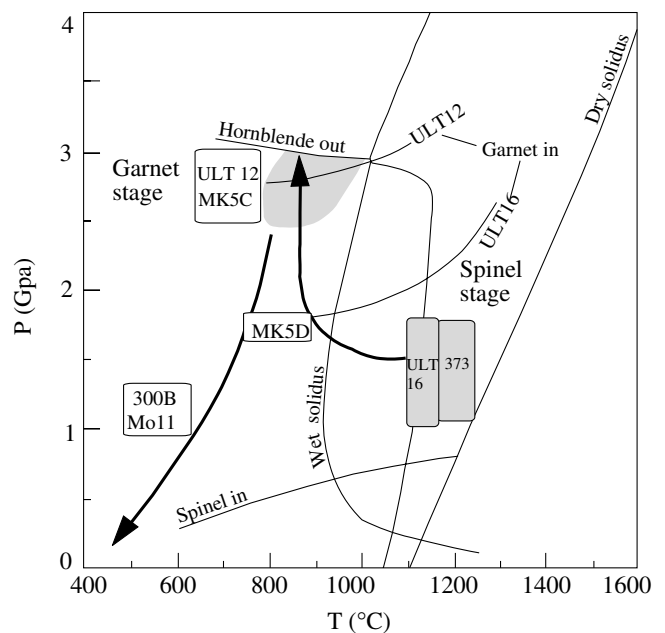

Fig. 1 Pressure–temperature evolution of the Ulten Zone peridotites. *Shaded boxes* labelled MK5D and ULT16 refer to the spinel-facies equilibration, whereas the garnet-in curves refer to formation of the amphibole + garnet assemblages. After Nimis and Morten (2000)

Preserved wedge-type spinel lherzolites (samples 373; ULT 16) These are coarse-grained protogranular to porphyroclastic rocks still retaining unaltered spinel-facies textures and assemblages and showing little signs of the garnet-facies recrystallization (Fig. 2a). Clinopyroxene and orthopyroxene display exsolution lamellae of orthopyroxene, clinopyroxene and spinel. Spinel also occurs as large grains. No primary amphibole has been detected in the spinel-facies assemblage. Late-stage retrograde Ca-amphibole locally replaces the rims of clinopyroxene and overgrows the exsolution lamellae. In sample ULT 16 rare garnet coronas overgrow spinel. In sample 373 olivine is partly serpentinized and this feature can be responsible for the relatively high loss on ignition (LOI) on whole rock analyses (Table 1).

Spinel peridotites with coronitic garnet (MK5D) The texture of this rock type is transitional between the relic spinel-peridotite and the foliated garnet–amphibole peridotite. MK5D is representative of a group of coarse-grained peridotites which preserve the protogranular to porphyroclastic spinel facies textures, although a new fabric progressively develops in these rocks. They display widespread coronitic overgrowths of garnet on spinel, well visible even at the mesoscale in the field. In thin section the relict spinel-facies assemblage mainly consists of porphyroclastic orthopyroxene and clinopyroxene, olivine and spinel. Garnet forms millimetre-thick coronas around spinel; it also occurs as exsolutions within pyroxenes and in granoblastic aggregates together with neoblastic pyroxene and olivine. Amphibole is rare and, when present, appears to replace clinopyroxene and garnet.

Amphibole + garnet mylonitic peridotites (MK5C, ULT 12) These are intensely deformed and display a foliation marked by amphibole. Olivine and orthopyroxene are often recrystallized and display a mosaic texture. ULT 12 has a fine-grained foliation with coexisting garnet, clinopyroxene, orthopyroxene, olivine and amphibole (Fig. 2b). Aggregates of undeformed (retrograde) amphibole around garnet are also present in this rock. Comparable textural features characterize sample MK5C, which belongs to the same outcrop of MK5D: it represents a highly deformed domain where complete syn-tectonic transformation of spinel (±coronitic garnet) lherzolite into garnet + amphibole peridotite obliterated all previous textures and assemblages. MK5C has a fine-grained foliation with clinopyroxene, orthopyroxene, olivine, amphibole and garnet; in addition, retrograde amphibole in this rock can also replace garnet and clinopyroxene. Compared with ULT 12, MK5C has a higher modal clinopyroxene and lower amphibole content (13 vol% amphibole in MK5C, 21 vol% in ULT12).

Amphibole-bearing mylonitic peridotites (MO11, 300B) They display an amphibole + orthopyroxene + olivine + spinel ± phlogopite assemblage. Former garnet and clinopyroxene were consumed during hydration and amphibole formation (Obata and Morten 1987; Rampone and Morten 2001). The modal amphibole content of these samples is around 20 vol%, quite comparable with that of ULT12. MO11 and 300B rarely preserve relics of former garnet and pyroxene (Nimis and Morten 2000), and pervasively recrystallized into new fine-grained aggregates of granoblastic orthopyroxene, amphibole and olivine. Phlogopite occurs only in sample 300B, where it is aligned along the mylonitic foliation.

Analytical techniques

The trace element compositions of bulk rocks and minerals were determined using laser ablation, inductively-coupled plasma mass spectrometry (LA ICP-MS) at the Research School of Earth Sciences (RSES), ANU. This technique employs an ArF (193 nm) EXCIMER laser and a Hewlett Packard Agilent 7500 quadrupole ICP-MS. With the exception of Li and Be, the bulk rock trace element analyses were performed on fused disks. To completely dissolve the accessory phases, the rock powders were fused with a flux of Li metaborate and Li tetraborate in the ratio of 3:1 (0.5 g sample and 1.5 g flux) at 1,200°C for 20 min. Bulk rock concentrations of

Fig. 2 a Pristine spinel lherzolite 373/3 showing fresh and unreacted spinel, olivine and orthopyroxene. b Garnet + amphibole peridotite ULT 12 showing syn-tectonic amphibole in textural equilibrium with garnet, olivine and pyroxenes of the eclogite-facies paragenesis
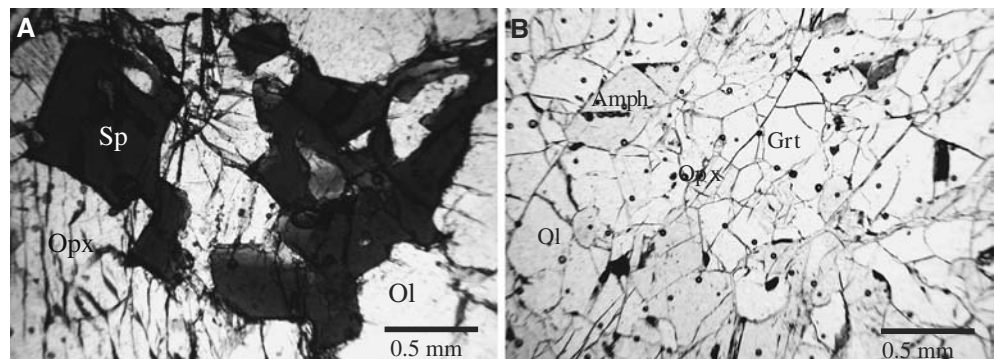
Table 1 Bulk-rock trace element concentrations in the Ulten peridotites

	373	ULT16	MK5D	MK5C	ULT12	MO11	300B
Li	1.85	3.32	2.01	3.14	2.99	2.69	4.18
Be	0.01	0.12	0.02	0.06	0.11	0.13	0.11
Cs	0.13	0.06	0.10	0.20	0.14	0.06	0.15
Rb	0.33	0.13	0.58	1.22	1.36	0.73	1.41
Ba	2.64	3.86	10.10	67.7	37.3	35.8	22.2
Pb	0.49	0.83	0.38	2.59	3.19	5.50	3.73
Th	0.02	0.04	0.05	0.62	0.12	0.11	0.24
U	0.03	0.04	0.03	0.14	0.10	0.14	0.19
Nb	0.09	0.11	0.14	0.66	0.53	0.87	0.46
P	128	140	130	119	143	130	135
La	0.21	0.43	0.16	2.42	0.65	0.97	1.77
Ce	0.24	0.80	0.14	4.32	1.60	2.60	2.87
Pr	0.05	0.11	0.02	0.49	0.26	0.41	0.34
Sr	3.74	3.99	5.58	33.1	24.7	42.2	21.7
Nd	0.15	0.37	0.12	1.69	1.15	1.80	1.16
Zr	0.66	1.50	0.49	3.95	7.83	11.1	1.63
Hf	0.03	0.07	0.05	0.11	0.25	0.35	0.09
Sm	0.07	0.11	0.09	0.29	0.31	0.44	0.23
Eu	0.05	0.05	0.05	0.08	0.11	0.14	0.11
Ti	289	311	336	233	583	459	250
Gd	0.12	0.18	0.22	0.24	0.39	0.44	0.19
Tb	0.03	0.05	0.05	0.05	0.07	0.07	0.04
Dy	0.20	0.31	0.37	0.27	0.47	0.45	0.20
Y	1.14	1.79	2.20	1.50	2.56	2.37	1.08
Er	0.16	0.24	0.29	0.21	0.31	0.28	0.15
Yb	0.18	0.26	0.33	0.22	0.35	0.29	0.18
Lu	0.04	0.05	0.06	0.04	0.06	0.05	0.04
Sc	13.6	16	15.3	13.4	16.7	16.2	14.6
LOI	1.84	0.66	0.62	1.76	0.81	2.3	1.46

Li and Be were made on fused rock powders obtained by passing a current of up to 8 A through a 0.3-mm-thick molybdenum strips in a sealed steel container. Five bars of argon pressure in the container prevented volatile element loss during melting and oxidation of iron. Rapid quenching was achieved by simultaneously turning off the current and dropping the argon pressure to 1 bar. The LA ICP-MS analyses of bulk rock glasses prepared following the above procedures, were done with a 187 μm laser spot; counting times were 45 s for the background and 80–120 s for the sample. ^{43}Ca and ^{29}Si were employed as internal standard isotopes based on previously measured bulk rock CaO and SiO$_2$ concentrations. The values shown in Table 1 derive from the average of three to four spot analyses of each sample. NIST 612 glass (Pearce et al. 1997) was used as the external standard and a BCR-2G glass was used as secondary standard. Reproducibility about the mean values of 6 analyses were between 0.5 and 4% relative (1σ) for the majority of elements. The average of this glass yielded trace element contents within 2–6 wt% of the certified values of this standard (Wilson 1997).

Mineral analyses were done at similar running conditions, with laser spots varying from 144 to 112 μm. ^{29}Si was employed as internal standard based on previously measured SiO$_2$ concentrations. The NIST 612 glass was used as external standard, assuming the composition given by Pearce et al. (1997). During the analytical runs of mineral phases we also analysed a NIST 610 glass as a secondary standard, which yielded trace element concentrations within 0.2–6% of the certified values. In particular, the results obtained are within 0.2–2.4% for Li; 1.1–2.6 for Be; 0.2–0.9 for Ce; 5.2–6% for U; 0.4–0.6% for Pb; 0.1–1.3 for Cs.

Results

Trace element bulk rock compositions

Our study presents a comprehensive trace element dataset of the investigated samples (Table 1). The rare earth element (REE) bulk rock compositions published previously (Obata and Morten 1987; Morten and Obata 1983; Rampone and Morten 2001) compare well with the REE dataset presented here. Figure 3 reports the REE (left side of the Figure) and other trace element compositions of all samples normalized to the Primitive Mantle (PM) (McDonough and Sun 1995). Samples are subdivided into spinel peridotites (373 and ULT16), peridotite with coronitic garnet (MK5D), garnet + amphibole peridotites (ULT12, MK5C) and amphibole-peridotites (MO11, 300B).

All samples display a decrease in heavy REE (HREE) with decreasing atomic number. Such a feature characterizes partially depleted peridotites and is in agreement with the variability of Al$_2$O$_3$, CaO and MgO, which indicate that the starting peridotite materials were affected by variable degrees of depletion (Rampone and Morten 2001). The selected sample set can therefore be referred to a depleted mantle source and for this reason
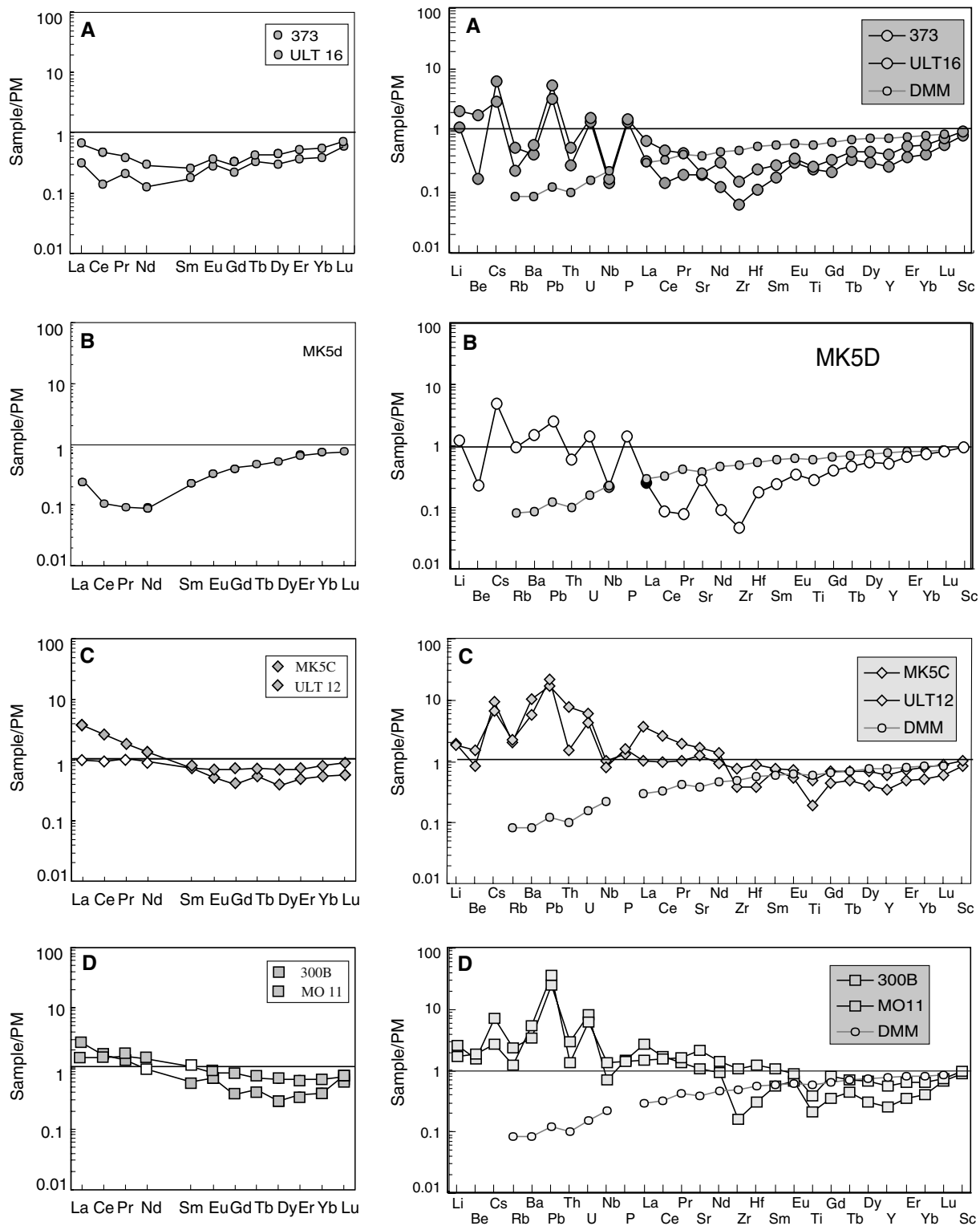
Fig. 3 Bulk-rock REE (*left side*) and trace element (*right side*) compositions of the analysed samples. Normalization to Primitive Mantle by McDonough and Sun (1995)

Fig. 3 also reports the composition of the depleted MORB Mantle (DMM; Workman and Hart 2005). In terms of decreasing CaO–Al$_2$O$_3$ and increasing MgO, the selected samples are as follows: MO11, 373, ULT 12, 300B, ULT16, MK5D, MK5C.

The spinel peridotites 373 and ULT16 are unaffected by garnet and amphibole crystallization and display very low absolute REE abundances, below the PM. Comparable features pertain to the coronitic sample MK5D, the garnet-bearing peridotite sample least affected by

hydration and amphibole crystallization. The REE patterns of these rocks are U-shaped, depleted in medium REE (MREE), and variably enriched in LREE. The amphibole ± garnet samples (Fig. 3c, d) have REE abundances around and below the PM: their REE patterns are rather flat for the HREE and MREE and display LREE enrichments above 1×PM. As outlined by Rampone and Morten (2001) this variability is unrelated with the degree of major element depletion, since the most fertile samples MO11 and 373 have lower REE abundances (LREE in particular) than the major element-depleted rock MK5C. It appears that all samples are variably affected by a metasomatic overprint leading to substantial LREE enrichment in both the amphibole-free spinel peridotites and the amphibole ± garnet peridotites.

The diagrams on the right hand side of Fig. 3 report the entire range of trace elements measured. A striking feature of all samples, spinel peridotites included, consists of the positive anomalies in LILE, particularly Cs, Pb and U. This is irrespective of the depletion in Al_2O_3 and CaO (e.g. sample MK5D), and the degree of enrichment is significant if compared with the DMM. For example, in the spinel peridotites 373 and ULT 16 it appears that besides Cs, Pb and U, other incompatible elements (e.g. Rb, Ba, Th, P) are enriched with respect to the DMM. The amphibole ± garnet rocks display higher Rb, Ba, Th than the spinel-peridotites and coronitic garnet one. Lithium is appreciably enriched (about 2×PM) in the majority of the peridotite samples analysed, whereas Be is slightly lower than the PM. The selected samples are affected by minor serpentinization and by formation of small modal amounts of retrograde tremolitic amphibole (see LOI in Table 1); hence some incompatible element enrichment (e.g. Li, Cs, Ba, Rb) might be in principle attributed to these retrograde phases.

Some of the above mentioned incompatible elements display positive correlations with the modal amphibole contents (estimates from Rampone and Morten 2001), featuring the income of water during crystallization of the garnet assemblages and at later stages. As an example, the Pb and Sr versus modal amphibole diagrams (Fig. 4) illustrate the coupled increase in such elements and water in the amphibole-bearing peridotites. Positive correlation trends are also defined by the incompatible element pairs Pb–Sr and Pb–U (Fig. 4). This indicates that the transition from dry spinel lherzolites to wet amphibole ± garnet peridotites was assisted by the influx of an aqueous fluid carrying incompatible trace elements.

Trace element mineral compositions

Spinel-bearing peridotites

The average compositions of rock-forming minerals in the spinel peridotites 373 and ULT 16 are shown in Table 2; all analyses are plotted in the PM-normalized diagrams of Figs. 5 and 6. Both samples contain clinopyroxene and orthopyroxene with spoon-shaped REE patterns, depleted in MREE and variably enriched in LREE. The REE abundances of orthopyroxene are below the PM, whereas clinopyroxene has higher absolute REE concentrations. The LREE enrichment is particularly emphasized in sample ULT16, La being as high as 2 and 10×PM in orthopyroxene and clinopyroxene, respectively (Fig. 6). The HREE abundances are around 1 and between 1 and 3×PM in orthopyroxene and clinopyroxene. Garnet sporadically forms thin coronitic rims around spinel in ULT 16: it shows typical HREE-enriched, MREE–LREE-depleted patterns. The HREE

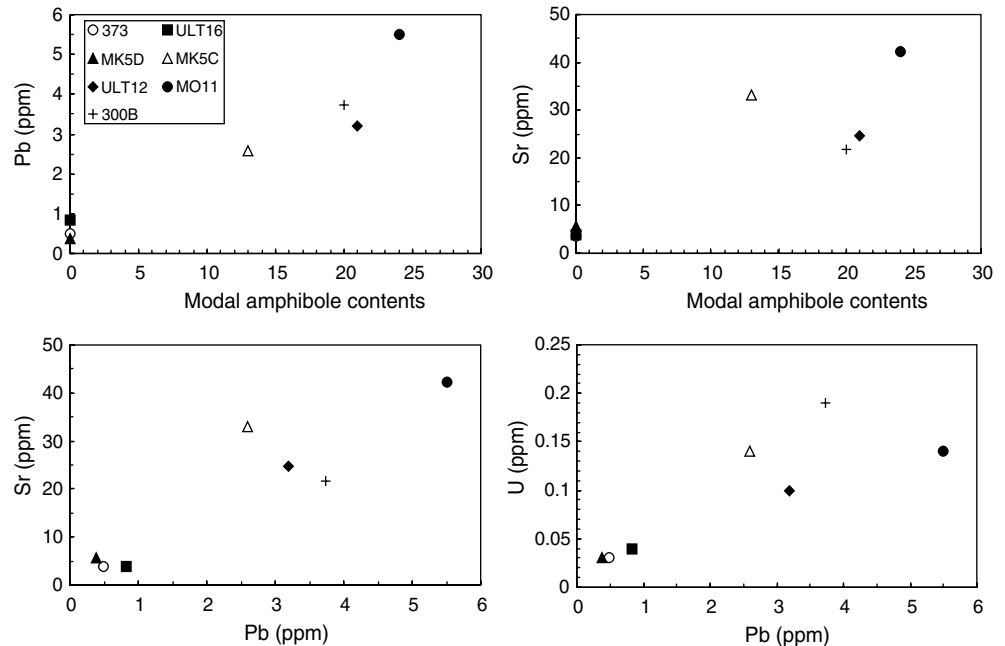Fig. 4 Bulk-rock variability of several fluid-mobile elements

Table 2 Trace element compositions of rock-forming minerals in the spinel lerzolites (373 and ULT16) and in the spinel peridotite with coronitic garnet (MK5D)

| Sample	373						ULT16									MK5D									
	opx (14)	SD	cpx (7)	SD	ol (7)	SD	opx (6)	SD	cpx (19)	SD	ol (6)	SD	gnt (4)	SD	amph (1)	opx (7)	SD	cpx (9)	SD	ol (11)	SD	gnt (5)	SD	amph (1)
Li	1.20	0.17	4.17	1.06	1.39	0.08	2.08	0.60	16.79	4.67	1.85	0.14	0.50	0.08	2.49	0.45	0.19	4.83	1.18	1.34	0.15	0.54	0.01	4.78
Be	0.01	0.002	0.03	0.005	0.21	0.05	0.05	0.01	0.20	0.09	0.02	0.003	0.0024	0.001	0.44	0.01	0.00	0.02	0.003	bd	–	0.001	0.0001	0.07
Cs	0.02	0.004	0.01	0.002	bd	–	0.01	0.003	0.02	0.02	0.02	0.01	0.025	0.006	0.129	0.02	0.01	0.01	0.004	0.01	0.01	0.02	0.01	0.17
Rb	0.03	0.01	0.06	0.05	0.02	0.006	0.02	0.01	0.04	0.03	0.21	0.13	0.22	0.07	6.38	0.03	0.01	0.02	0.004	bd	–	0.82	1.09	0.23
Ba	0.04	0.02	0.17	0.09	bd	–	1.07	0.64	2.60	1.68	0.01	0.003	0.09	0.03	675	0.40	0.14	0.62	0.49	0.50	0.36	0.11	0.11	14.03
Pb	0.06	0.02	0.32	0.10	0.03	–	0.51	0.46	1.03	0.84	0.005	0.002	0.09	0.08	8.57	0.03	0.02	0.45	0.04	0.49	0.29	0.32	0.25	1.20
Th	0.01	0.004	0.02	0.004	bd	–	0.16	0.08	0.22	0.04	0.005	0.002	0.13	0.09	0.76	0.05	0.03	0.17	0.02	0.02	0.00	0.08	0.03	0.39
U	bd	–	0.01	–	bd	–	0.03	0.01	0.06	0.01	0.005	0.002	0.04	0.03	0.58	0.01	0.002	0.10	0.01	0.02	0.01	0.04	0.01	0.21
Nb	0.06	0.02	0.07	0.01	bd	–	0.15	0.07	0.10	0.03	0.002	0.001	0.04	0.002	4.63	0.01	0.002	0.05	0.01	0.005	0.005	0.04	0.01	1.00
Ta	0.01	0.003	0.02	0.010	bd	–	0.01	0.002	0.01	0.002	bd	–	bd	–	0.23	bd	–	0.01	0.01	bd	–	bd	–	bd
P	7.61	0.90	9.55	1.27	12.7	1.20	7.49	0.54	8.60	0.58	13.15	3.68	37.1	4.33	57.5	6.8	1.0	8.13	0.66	13.3	1.5	35.1	1.7	29.61
La	0.03	0.01	1.03	0.16	0.01	0.001	0.18	0.08	4.66	0.48	0.01	0.002	0.004	0.001	10.3	0.01	0.001	0.84	0.11	0.003	0.0004	0.01	0.00	1.57
Ce	0.05	0.01	2.70	0.44	0.04	0.02	0.28	0.20	10.6	0.92	0.01	0.003	0.01	0.003	26.2	0.004	0.003	0.56	0.13	0.003	0.002	0.01	0.00	1.16
Pr	bd	–	0.36	0.06	bd	–	0.021	0.015	1.03	0.09	bd	–	bd	–	3.08	0.001	0.0003	0.05	0.01	0.001	0.0003	0.002	0.001	0.09
Sr	0.29	0.10	26.3	2.44	0.10	0.04	0.65	0.47	26.6	1.54	0.01	0.01	0.01	0.006	187	0.04	0.03	3.03	0.43	0.36	0.14	0.03	0.02	4.05
Nd	0.02	0.01	1.64	0.28	0.01	0.003	0.06	0.04	3.04	0.23	bd	–	0.05	0.01	10.6	0.01	0.001	0.58	0.04	0.47	0.67	0.06	0.06	0.95
Zr	0.36	0.11	6.66	0.94	0.01	0.01	0.50	0.16	9.05	1.01	0.01	0.01	1.02	0.07	17.1	0.04	0.02	1.24	0.10	0.02	0.01	1.04	0.11	1.92
Hf	0.01	0.003	0.16	0.017	bd	–	0.02	0.01	0.32	0.03	bd	–	0.07	0.00	0.53	0.01	0.001	0.23	0.02	0.002	0.001	0.06	0.01	0.27
Sm	0.01	0.002	0.67	0.11	bd	–	0.01	0.01	0.65	0.05	bd	–	0.18	0.01	1.86	0.01	0.002	0.54	0.04	0.004	0.001	0.18	0.04	0.98
Eu	bd	–	0.28	0.05	bd	–	0.01	0.003	0.23	0.02	bd	–	0.14	0.01	0.45	0.002	0.001	0.21	0.01	0.001	0.0003	0.15	0.01	0.38
Ti	466	55	1,808	290	22.2	6.17	361	52.3	1,262	76	19.98	5.61	434	44.0	1,508	409	78	1,449	217	15	9	401	41.0	3,827
Gd	0.02	0.01	1.10	0.18	bd	–	0.03	0.01	1.00	0.08	bd	–	0.98	0.10	1.42	0.01	0.003	0.85	0.06	bd	–	1.21	0.10	1.61
Tb	bd	–	0.22	0.03	bd	–	0.01	0.003	0.20	0.02	bd	–	0.27	0.04	0.19	0.003	0.0003	0.12	0.01	bd	–	0.41	0.07	0.26
Dy	0.04	0.01	1.69	0.25	bd	–	0.06	0.03	1.59	0.13	bd	–	2.43	0.48	1.23	0.01	0.004	0.64	0.04	0.01	0.01	4.42	1.11	1.73
Y	0.30	0.08	9.96	1.42	0.01	0.004	0.43	0.21	9.71	0.77	0.003	0.001	15.43	3.78	6.65	0.07	0.02	2.35	0.22	0.06	0.04	34.4	11.4	8.38
Er	0.05	0.01	1.16	0.16	bd	–	0.07	0.03	1.15	0.09	bd	–	1.85	0.54	0.73	0.01	0.002	0.21	0.04	0.01	0.01	4.70	1.72	0.92
Yb	0.11	0.02	1.16	0.14	bd	–	0.13	0.05	1.15	0.10	bd	–	2.05	0.58	0.77	0.01	0.002	0.13	0.05	0.01	0.01	6.01	2.60	0.83
Lu	0.02	0.004	0.17	0.02	bd	–	0.02	0.01	0.17	0.01	bd	–	0.31	0.08	0.12	bd	–	0.01	0.01	bd	–	0.77	0.06	0.11
Sc	18	1.59	72	5.07	2.70	0.20	14.8	2.67	67	2.9	1.98	0.12	98.00	3.29	47.6	5.68	0.58	35.5	1.59	1.9	0.2	122	10.75	50.88
Cr	2,461	530	6,453	701	11.3	0.95	4,293	2,178	6,098	1,037	18.71	3.12	5,079	260	5,914	1,775	487	5,321	328	24	7	6,216	2,120	5,911
Ni	553	36.95	370	29	2,859	30	732	41	435	30	2,876	142	12	3	672	570	24	276	12	2,897	40	14	2	1,157
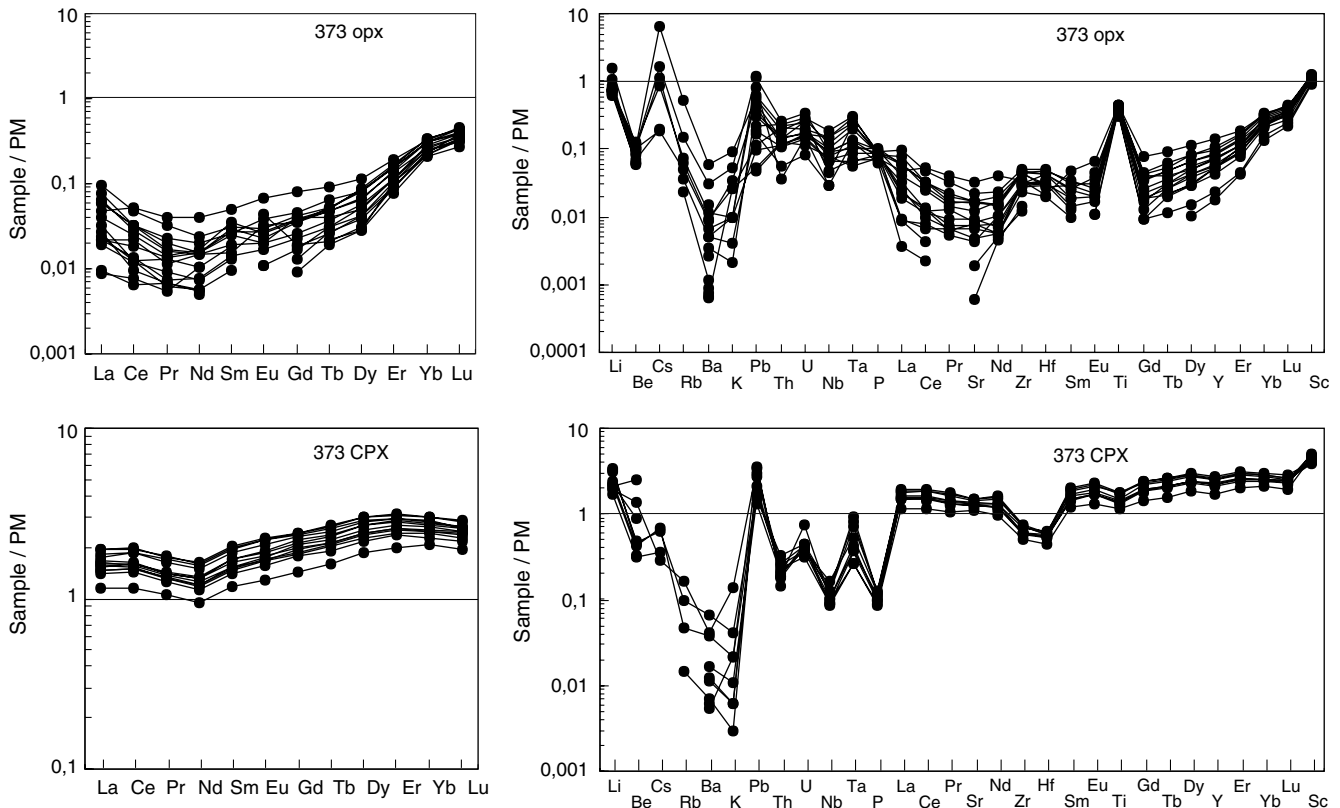
Fig. 5 Rare earth element and trace element compositions of pyroxenes of the spinel peridotite sample 373

contents of orthopyroxene and clinopyroxene are relatively high and do not reflect equilibration with garnet, which would lead to much lower HREE contents in pyroxenes (about 100 times lower than garnet). This indicates a lack of equilibrium between pyroxenes and garnet and suggests that the LREE enrichment in the spinel-facies minerals pre-dates garnet formation.

The trace element patterns of orthopyroxene and clinopyroxene display positive spikes in Li, Pb and U. Clinopyroxene also shows a slight enrichment in Ta with respect to Nb. The Pb_N/Nb_N ratio in clinopyroxene, representing the LILE/HFSE fractionation, ranges from 16 to 51 in sample 373, and from 17 to 90 in ULT 16: the respective average values are 27 and 40. Ranges of Ce/Pb ratios in clinopyroxene are 6–13 in sample 373 and 3–25 in ULT16. Relatively high Li contents were measured in orthopyroxene (1.3–4.2 ppm; i.e. 3×PM) and in clinopyroxene (3–23 ppm; i.e. above 15×PM). The spinel-facies clinopyroxene has normalized Li higher than Be (Figs. 5, 6). Olivine has Li and P contents in the range of 1–3 ppm and around 15 ppm, respectively. Retrograde amphibole in ULT16 has REE spectra similar to the ones of clinopyroxene at slightly higher absolute concentrations. This amphibole hosts appreciable Rb and Ba; a representative analysis is reported in Table 2.

The similar trace element patterns of pyroxenes in sample 373 and ULT16, as well as the lack of trace element equilibrium between small coronitic garnet and porphyroblastic pyroxenes, provide evidence that the

trace element signature of pyroxenes was acquired during the high temperature equilibration in the spinel-peridotite field.

Spinel peridotites with coronitic garnet (MK5D)

This contains clinopyroxene (Fig. 7), which has unusual features and significantly differs from both the spinel-facies clinopyroxene in 373 and ULT16, and the clinopyroxene that fully equilibrated with garnet in MK5C and ULT12 (Figs. 8, 9). The MK5D clinopyroxene has a saddle-shaped REE pattern, depleted in HREE and some MREE, and enriched in LREE. The HREE depletion in this unique pattern clearly reflects equilibration with garnet, which is HREE-enriched. On the other hand, the depletion in Nd and Pr and the enrichment in La and Ce are not easily comparable with other clinopyroxene patterns. The LREE enrichment of the MK5D clinopyroxene is quite different from those of the other garnet-facies clinopyroxenes and may reflect two main processes: (1) the inheritance of a LREE enrichment occurred during a previous spinel-facies equilibration (cf. with the ULT16 clinopyroxene); (2) a LREE input during garnet crystallization.

In terms of incompatible trace elements, clinopyroxene is enriched in Pb, Th, U, and has normalized Pb_N/Nb_N values between 29 and 92, with an average value of 51. Average Pb_N/Nb_N in orthopyroxene is 36. Normalized
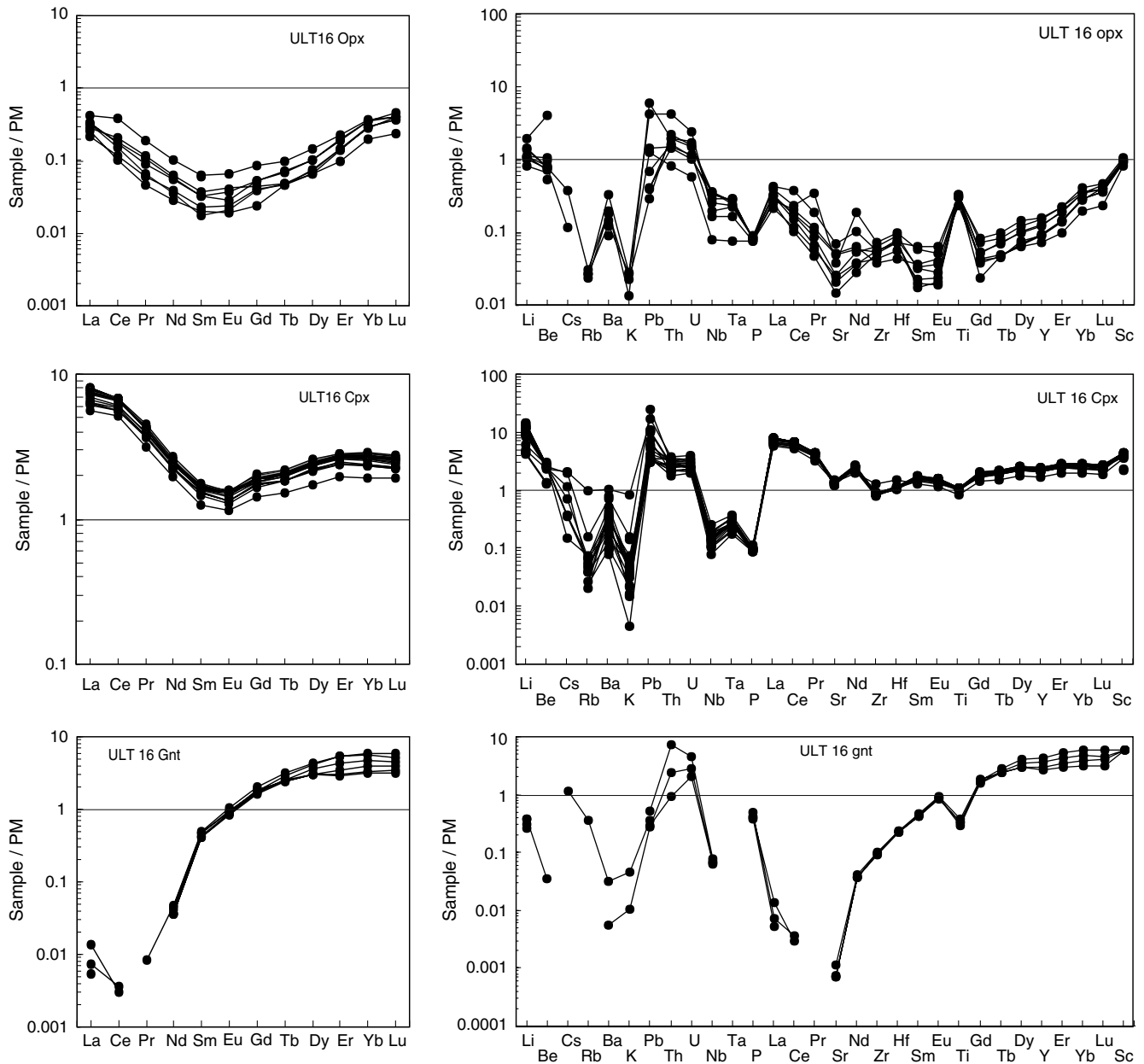
Fig. 6 Rare earth element and trace element compositions of minerals of the spinel peridotite sample ULT16

Li in clinopyroxene is higher than Be, a feature comparable to what is observed in the spinel-facies pyroxenes. Retrograde amphibole displays about a factor of two higher trace element concentrations than clinopyroxene, apart from the HREE which are nearly ten times higher. The high HREE suggest that the analysed amphibole is not in equilibrium with garnet and hence it might have formed during later retrogression.

Amphibole + garnet mylonitic peridotites (MK5C, ULT 12)

These contain garnet, clinopyroxene and amphibole in textural equilibrium (Table 3). MK5C outcrops in continuity with MK5D and represents a highly deformed and hydrated end-member, characterized by significant amphibole crystallization. The LREE contents of MK5C clinopyroxene is up to 10×PM (Fig. 8): the saddle-shaped pattern of MK5D clinopyroxene is no longer detected and clinopyroxene has LREE-enriched and HREE-depleted compositions. MK5C orthopyroxene has a REE pattern slightly enriched in LREE; compared with the spinel-facies one, this orthopyroxene has much lower HREE, between 0.1 and 0.01×PM. Pyroxenes in these samples thus fully equilibrated with the eclogite-facies garnet. Amphibole has LREE-enriched patterns, with La up to 10–30×PM. Two amphibole groups are distinguished in MK5C based on the texture
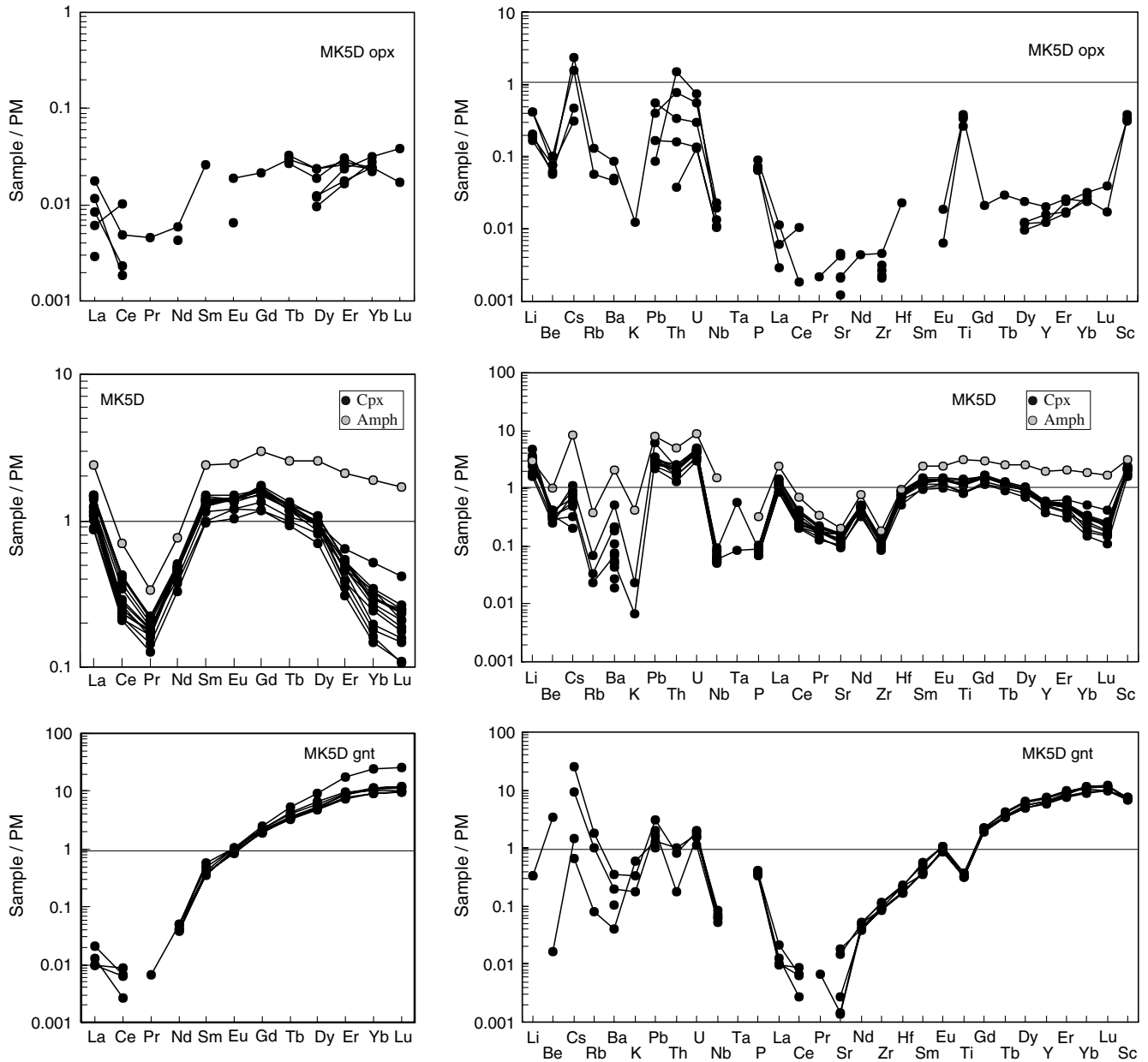
Fig. 7 Rare earth element and trace element compositions of minerals of the spinel peridotite with coronitic garnet MK5D

and on the REE abundances: (1) one (along the mylonitic foliation; full dots in Fig. 8) with flat HREE, about 2×PM; (2) one (in patches around garnet; white dots in Fig. 8) with higher HREE, showing increasing HREE content with increasing atomic number. The latter pattern is typical of amphibole replacing garnet and incorporating its high HREE contents. The first amphibole pattern does not show equilibrium partitioning with garnet and clinopyroxene because it has far too high HREE contents. This indicates that even the mylonitic amphibole in textural equilibrium with garnet and clinopyroxene shows a retrograde HREE re-equilibration during partial garnet breakdown.

ULT 12 contains clinopyroxene and orthopyroxene that display low HREE contents, indicative of coexis-

tence with garnet (Fig. 9). Accordingly, the syn-tectonic amphibole, which coexists with garnet, pyroxenes and olivine along the mylonitic foliation also shows also low HREE contents (0.3–0.5×PM). In contrast; as observed in sample MK5C, rims of syn-tectonic amphibole, and static retrograde amphibole overgrowths around garnet are characterized by higher HREE contents (1–3×PM). Thus, ULT 12 is the only sample still retaining equilibrium compositions among the five-phase assemblage garnet, orthopyroxene, clinopyroxene, olivine and amphibole.

Clinopyroxene in the amphibole + garnet peridotites is enriched in Li, Be, Cs, Ba, Pb, U. It also displays high Pb_N/Nb_N (330–615) and low Ce/Pb (1.39–2.66), compared with the spinel-facies clinopyroxenes. Another
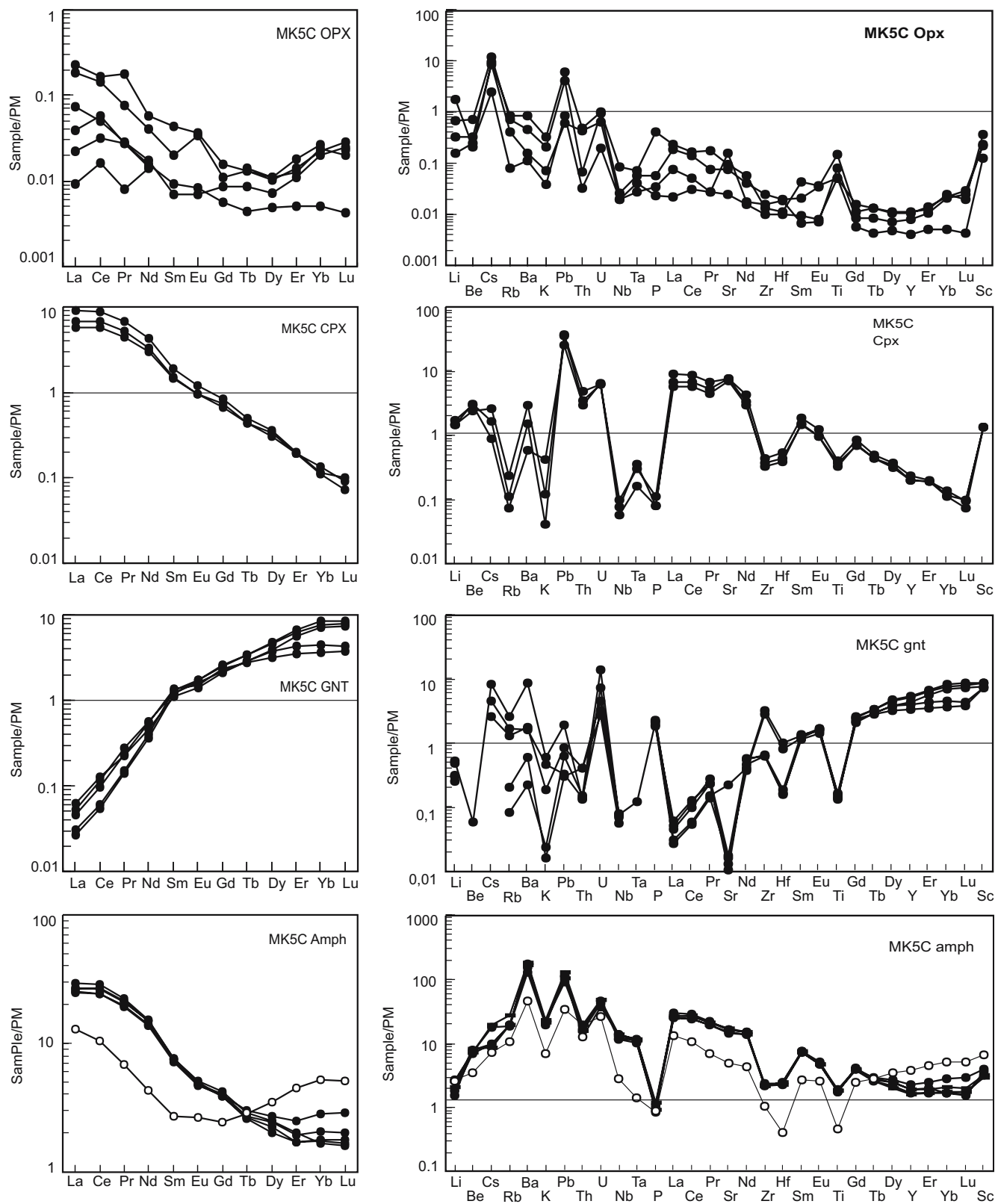
Fig. 8 Rare earth element and trace element compositions of minerals of the amphibole + garnet peridotite MK5C. The *different symbols* refer to two observed amphibole groups, mylonitic amphibole (*full dots*) and retrograde amphibole (*white dots*)
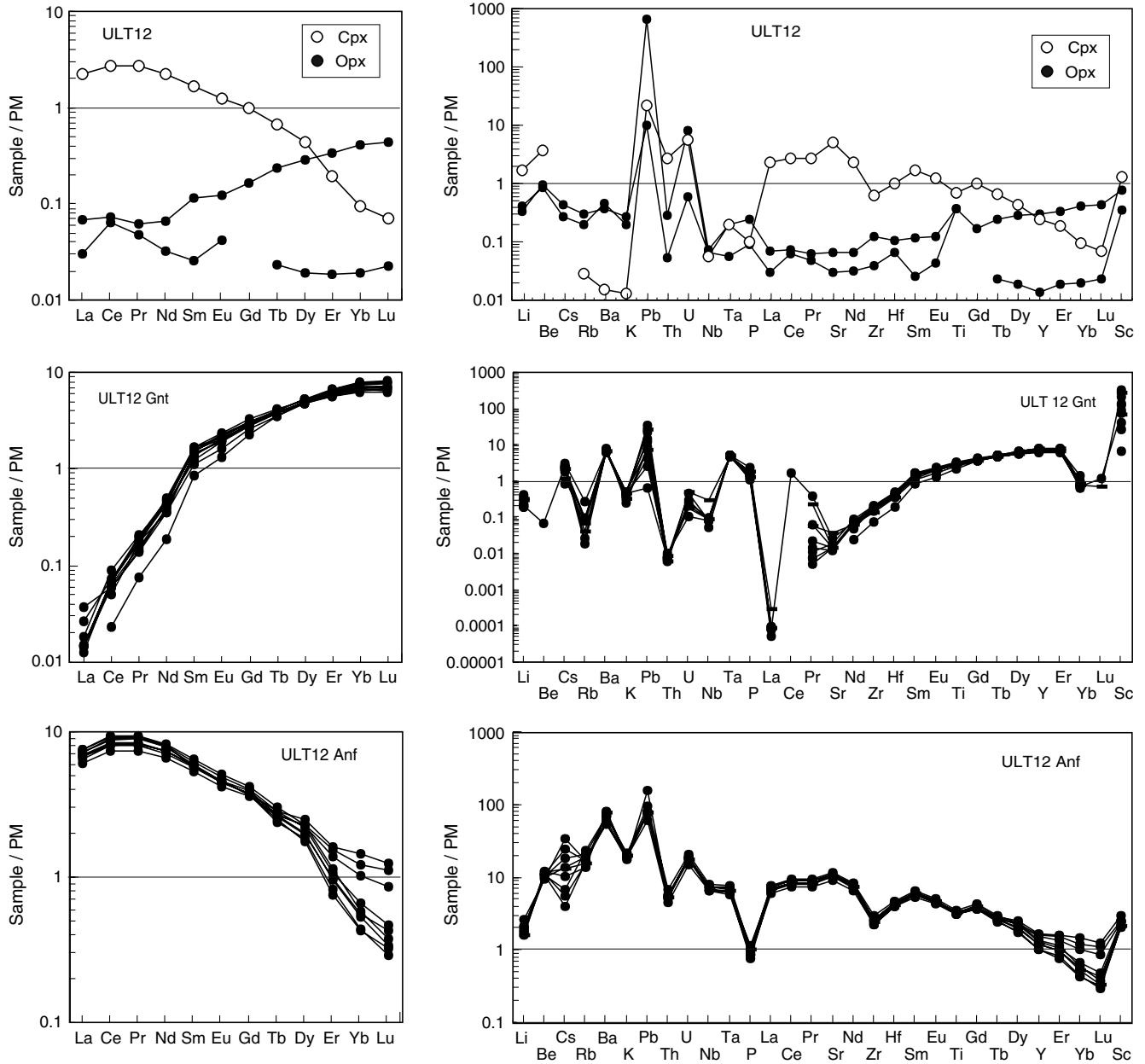
Fig. 9 Rare earth element and trace element compositions of minerals of the amphibole + garnet peridotite ULT12

change in the garnet-facies clinopyroxene concerns the Li–Be variability, as clinopyroxenes of ULT12 and MK5C have normalized Li higher than Be. Olivine has Li and P between 3–4.5 and 40–70 ppm, respectively.

Amphibole mylonitic peridotites MO11 and 300B (Fig. 10)

They do not preserve garnet and clinopyroxene and contain an orthopyroxene + olivine + amphibole + spinel ± phlogopite assemblage. The amphibole compositions in both samples are quite similar to those of MK5C and have HREE above 1×PM, suggesting disequilibrium with former garnet (Table 4). The amphibole 300B is richer in HREE, LREE, Li and Cs (Fig. 10) than MO11 amphibole. Similarly, orthopyroxene displays significant difference in LREE concentrations, with 300B orthopyroxene being one order of magnitude richer than orthopyroxene in MO11.

Phlogopite was only observed in sample 300B and displays the highest concentrations in LILE (more than 1,000×PM Cs, Rb, Ba). This indicates that phlogopite formation is related to influx of a potassium and LILE bearing aqueous fluid. The Nb and Ta contents (up to 10×PM) are relatively low compared with the above
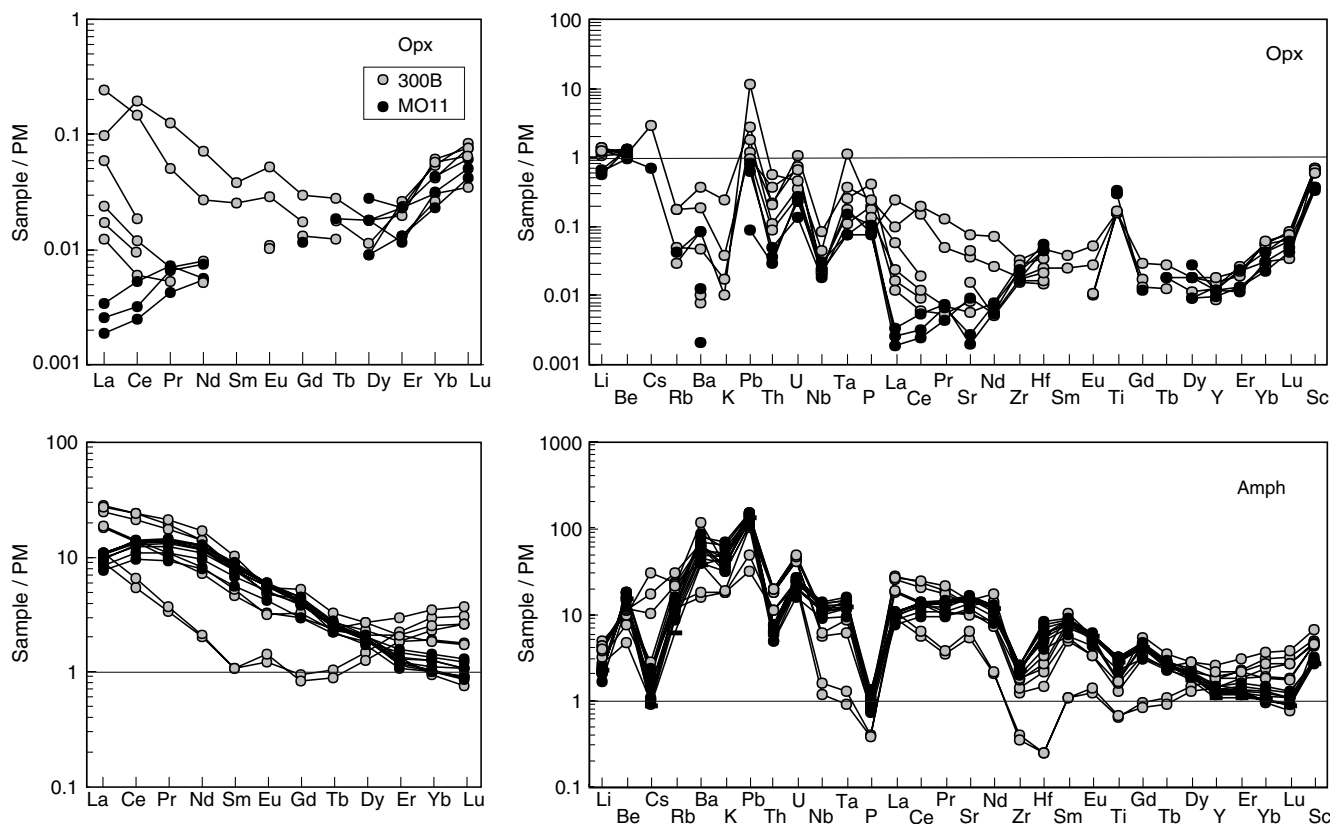
Fig. 10 Rare earth element and trace element compositions of minerals of the amphibole peridotites MO11 and 300B

LILE (Tables 2, 3, 4), whereas the REE contents are very low and often below detection. Li and P in olivine range between 3–6 and 30–60 ppm, respectively.

In summary, minerals of the whole sample set are enriched in incompatible elements, particularly in U, Pb, Cs and Li. Relevant Ba, K and Rb contents are hosted by various generations of amphiboles. As a general tendency, all mineral phases are relatively depleted in the HFSE Nb, Ta, Zr, Hf with respect to LREE, LILE and light elements. The spinel-facies clinopyroxene has high Li and Pb and displays variable enrichments in U and Th (Figs. 5, 6); it has normalized Li higher than Be. Such an imprint is shared by the coexisting orthopyroxene (Figs. 5, 6), whereas the spinel-facies olivine appears enriched in Li and Pb, compared with the other LILE (Table 1). In the garnet-facies samples, clinopyroxene has Li, Pb, Th, U significantly higher than 1×PM, and displays normalized Be higher than Li. Orthopyroxene shows progressive enrichment in incompatible elements at the left hand of spider-diagrams in Figs. 8 and 9, with positive spikes in Li, Cs, Pb and U. Amphibole with low HREE in geochemical equilibrium with garnet (ULT 12) has the same Li-Be fractionation as clinopyroxene and tends to concentrate Rb, Ba and K, which are very low in pyroxenes. The Pb–Th–U patterns are quite similar in both phases. The concentrations of most trace elements in olivine are below the detection limit, with the exception of Ni, Cr, Ti, Li and

P. The most interesting feature in olivine concerns the systematic change of Li and P contents according to different metamorphic stages of the peridotite (Fig. 11). The transition from spinel to amphibole $\pm$ garnet peridotites is accompanied by an abrupt coupled increase of P and Li contents of olivine. Within the amphibole $\pm$ garnet peridotites, Li in olivine increases from the amphibole + garnet samples ULT12 and MK5C, to the amphibole-peridotites MO11 and 300B. This indicates that Li in olivine is partly incorporated via a coupled substitution, in which Li and P replace Mg and Si, respectively.

Discussion

Distribution of Li and other trace elements
in the spinel- and in the garnet-facies peridotites

As a whole, the investigated samples display evidence of metasomatic modification during their evolution. In order to establish when the metasomatic imprint was achieved, it is crucial to determine the major hosts of trace elements. This information, combined with the known stability field of key minerals such as spinel, garnet and amphibole provides constraints on the metamorphic conditions at which metasomatism occurred. We have chosen the spinel peridotite ULT16 and

386

Table 3 Trace element compositions of rock-forming minerals in the garnet + amphibole peridotites MK5C and ULT12

Sample	MK5C										ULT12											
	opx (4)	SD	cpx (3)	SD	ol (11)	SD	gnt (5)	SD	amph (5)	SD	opx (3)	sD	cpx (1)	SD	ol (5)	gnt (11)	SD	amph1 (3)	SD	amph2 (6)	SD
Li	1.15	1.12	2.46	0.29	3.68	0.35	0.60	0.20	3.40	0.74	0.60	0.10	2.67	0.48	3.47	0.41	0.12	3.22	0.89	3.03	0.32
Be	0.03	0.02	0.19	0.02	bd	0.00	bd	–	0.51	0.04	0.06	0.003	0.25	–	bd	0.005	0.001	0.69	0.05	0.75	0.04
Cs	0.17	0.08	0.04	0.02	0.03	0.01	0.11	0.06	0.27	0.10	0.01	0.002	bd	–	bd	0.04	0.01	0.50	0.21	0.20	0.11
Rb	0.30	0.20	0.08	0.05	0.05	0.02	0.70	0.63	12.5	2.17	0.15	0.04	0.02	0.020	0.04	0.17	0.09	10.5	0.70	10.3	2.14
Ba	3.20	2.32	11.1	7.95	0.40	0.10	6.90	4.96	1,062	146	2.70	0.41	0.10	0.14	0.29	0.51	0.80	377	25	484	33.48
Pb	0.43	0.39	4.84	0.91	0.19	0.07	0.12	0.10	16.4	2.03	1.52	0.45	3.31	–	0.18	1.88	1.56	14.8	7.69	12.1	1.00
Th	0.02	0.02	0.29	0.08	0.02	0.01	0.02	0.01	1.27	0.20	0.004	0.00	0.21	–	bd	bd	–	0.40	0.04	0.44	0.05
U	0.02	0.01	0.15	0.003	0.01	0.01	0.14	0.10	1.02	0.10	0.01	0.00	0.13	0.01	bd	0.04	0.01	0.38	0.05	0.43	0.03
Nb	0.02	0.02	0.05	0.01	0.07	0.01	0.05	0.01	8.55	0.71	0.04	0.004	0.04	–	0.03	0.07	0.04	4.49	0.28	4.74	0.34
Ta	0.002	0.001	0.01	0.004	bd	–	0.004	0.00	0.40	0.02	0.005	0.002	0.01	–	bd	0.03	0.01	0.23	0.02	0.26	0.02
P	3.44	1.57	8.18	1.65	59.7	6.99	184	17	91.8	11.6	8.03	2.53	9.09	8.57	57.77	191	58	75	5	90	8.60
La	0.08	0.06	4.70	1.13	0.02	0.02	0.03	0.01	17.3	1.09	0.03	0.00	1.47	–	bd	0.01	0.01	4.19	0.25	4.67	0.20
Ce	0.16	0.11	11.8	2.62	0.01	0.002	0.15	0.06	43.8	2.99	0.11	0.01	4.60	0.01	0.01	0.11	0.03	13.1	0.68	14.8	0.77
Pr	0.02	0.02	1.38	0.29	0.01	0.004	0.05	0.01	5.24	0.31	0.01	0.002	0.69	–	bd	0.04	0.01	1.99	0.11	2.26	0.12
Sr	1.74	1.08	147	7.43	0.27	0.16	0.28	0.06	318	25	0.97	0.52	102	0.04	0.05	0.26	0.25	193	15.1	213	10.97
Nd	0.04	0.02	4.40	0.81	0.03	0.002	0.58	0.11	18.2	0.89	0.06	0.03	2.83	0.00	0.002	0.50	0.10	8.75	0.48	9.74	0.46
Zr	0.16	0.07	3.92	0.63	0.03	0.02	16.2	13	23.1	0.59	0.83	0.59	6.35	0.01	0.04	15.65	3.60	24.5	2.51	26.4	2.06
Hf	0.004	0.001	0.13	0.02	0.02	0.01	0.13	0.12	0.67	0.03	0.02	0.01	0.29	–	bd	0.23	0.06	1.15	0.07	1.21	0.08
Sm	0.01	0.01	0.66	0.10	bd	–	0.50	0.04	3.03	0.08	0.03	0.03	0.67	–	bd	0.57	0.10	2.26	0.11	2.44	0.12
Eu	0.003	0.002	0.16	0.02	bd	–	0.24	0.02	0.75	0.03	0.01	0.01	0.19	–	bd	0.31	0.04	0.67	0.02	0.73	0.04
Ti	99	55	442	45	28.9	9.93	177	16	2,194	91	449	3.96	817	15.61	47.40	497	93	3,780	210	3,926	143
Gd	0.01	0.002	0.41	0.04	bd	–	1.28	0.11	2.17	0.06	bd	–	0.53	0.001	0.01	1.57	0.15	2.02	0.05	2.11	0.12
Tb	bd	–	0.045	0.003	bd	–	0.30	0.03	0.27	0.02	0.002	0.00	0.07	–	bd	0.38	0.02	0.27	0.01	0.26	0.02
Dy	0.01	0.002	0.23	0.02	0.01	0.00	2.72	0.42	1.60	0.17	0.01	0.002	0.30	0.00	0.02	3.33	0.12	1.57	0.10	1.35	0.14
Y	0.04	0.01	0.90	0.07	0.004	0.002	19.0	3.60	8.12	1.10	0.06	0.01	1.05	0.001	0.004	21.43	0.94	6.85	0.39	5.05	0.62
Er	bd	–	0.09	0.002	bd	–	2.30	0.59	0.86	0.14	0.01	0.00	0.08	0.004	0.01	2.70	0.16	0.66	0.05	0.42	0.06
Yb	0.01	0.004	0.05	0.01	0.01	0.001	2.75	0.90	0.88	0.21	0.01	0.00	0.04	0.005	0.02	3.12	0.22	0.54	0.09	0.24	0.04
Lu	0.001	0.001	0.01	0.001	bd	–	0.43	0.15	0.13	0.04	0.01	–	bd	–	bd	0.48	0.04	0.07	0.01	0.02	0.001
Sc	3.82	1.63	21.9	0.10	2.41	0.46	128	11	55.3	6.91	5.75	2.02	20.5	0.35	1.74	109	6.34	42.3	4.42	35.8	3.20
Cr	514	143	1,632	544	19.3	8.53	8,809	1,020	8,464	613	1,268	400	2,211	4.38	18	8,923	1,304	7,896	563	9,231	1,329
Ni	570	642	291	14.9	2,877	38	10.44	2.32	792	30	568	23	317	145	3,104	14.72	2.03	832	85	835	17

Table 4 Trace element compositions of rock-forming minerals in the amphibole peridotites 300B and MO11

Sample	300B								MO11					
	opx (6)	SD	ol (7)	SD	amph (7)	SD	phlog (6)	SD	opx (4)	SD	ol (6)	SD	amph (9)	SD
Li	1.82	0.18	4.79	0.86	5.54	1.11	42.0	5.06	1.02	0.1	4.7	0.55	3.38	0.35
Be	0.07	0.01	bd	–	0.62	0.18	0.29	0.03	0.08	0.01	bd	–	1.10	0
Cs	0.06	0.02	bd	–	0.20	0.24	64.2	2.34	0.01	0.0	bd	–	0.03	0
Rb	0.06	0.05	bd	–	12.3	3.72	518	31.9	0.03	0	0.02	0.006	6.80	1.81
Ba	1.14	0.97	0.02	0.01	360	225	18,215	1,466	0.20	0.2	0.41	0.37	387	115
Pb	bd	–	0.014	0.007	15.1	6.76	58.3	2.48	0.06	0.05	0.04	0.02	20.1	2.09
Th	0.02	0.01	bd	–	1.34	0.31	7.01	1.87	0.003	0.001	bd	–	0.50	0
U	0.01	0.01	bd	–	0.90	0.26	0.10	0.05	0.005	0.002	0.002	0.001	0.52	0
Nb	0.02	0.02	0.04	0.02	4.35	2.77	8.83	0.20	0.02	0.005	0.122	0.03	8.00	0.94
Ta	0.01	0.00	0.02	0.01	0.30	0.20	0.59	0.01	0.004	0.002	bd	0	0.48	0.07
P	21.0	9.4	44.78	11.33	72.5	28.6	7.83	1.23	7.59	1.16	54.3	8.85	87	16.5
La	0.03	0.02	bd	–	12.7	4.96	0.06	0.007	0.002	0.001	0.005	0.003	6.45	0.71
Ce	0.16	0.15	0.02	0.01	26.2	13.1	0.01	0.004	0.006	0.002	0.031	0.02	21.3	2.51
Pr	0.01	0.01	bd	–	3.15	1.87	0.02	0.01	bd	–	0.005	0	3.30	0.43
Sr	0.71	0.55	0.04	0.03	209	69	138	8	0.05	0.01	0.128	0.11	299	29.5
Nd	0.03	0.04	bd	–	11.6	7.52	0.02	0.006	0.01	0.001	0.015	0.01	14.2	1.99
Zr	0.22	0.07	0.01	0.003	12.7	6.38	0.56	0.01	0.22	0.03	0.04	0.02	23.8	2.10
Hf	0.01	0.001	bd	–	0.49	0.33	0.06	0.005	0.01	0.001	bd	–	1.74	0.40
Sm	0.01	0.002	bd	–	2.24	1.45	bd	–	bd	–	0.002	0.001	3.21	0.43
Eu	bd	–	bd	–	0.54	0.27	0.27	0.02	bd	–	bd	–	0.87	0.09
Ti	194	4.89	25.92	6.57	1,583	581	5,429	497	368	33	58	14	3,491	406
Gd	0.01	0.00	bd	–	1.70	0.93	0.74	0.03	0.01	0.001	bd	–	2.22	0.25
Tb	bd	–	bd	–	0.22	0.09	bd	–	bd	–	bd	–	0.25	0.02
Dy	0.01	0.001	bd	–	1.42	0.39	bd	–	0.01	0.006	bd	–	1.30	0.08
Y	0.06	0.01	bd	–	7.84	1.71	1.77	0.15	0.05	0.005	bd	–	5.38	0.50
Er	0.01	0.00	bd	–	0.90	0.23	bd	–	0.007	0.002	bd	–	0.56	0.07
Yb	0.02	0.01	bd	–	1.01	0.38	0.01	0.000	0.02	0.004	bd	–	0.51	0.07
Lu	bd	–	bd	–	0.16	0.07	0.01	0.001	0.004	0.0006	bd	–	0.07	0.01
Sc	10.6	0.66	2.44	0.08	78.3	14.4	4.13	0.69	5.71	0.35	1.66	0.09	45.1	2.26
Cr	1,295	639	58.39	94	5,633	805	3,917	259	1,015	142	24.9	9.32	8,379	833
Ni	555	59	3,001	57	810	54	1,440	26	534	30	2,957	58	798	27

the garnet–amphibole peridotite ULT12 as representative samples for mass balance calculations. ULT16 contains a small volume percent of garnet (max 1% volume) in disequilibrium with the main rock-forming assemblage: garnet crystallization thus scarcely affected the original, spinel-facies imprint of this sample, which can be used to gain insights on trace element distribution among the dominant spinel-facies minerals. We used the modal abundance of minerals given in Rampone and Morten (2001) and the average trace element compositions given in Table 2 to calculate the contribution of each phase to the measured bulk rock (Table 1). The result for a selected series of trace elements is shown in Fig. 12. Generally, the sum of all mineral contributions to the measured bulk-rock trace element concentrations is between 80 and 120%, which is very reasonable considering the errors on the single minerals and the variation of multiple mineral analyses. In some cases the sum of mineral contributions exceeds 120%, and they have been normalized to 100% for better visualization of the main trends (see the caption of Fig. 12 for details).

In the spinel peridotite ULT16, the REE, Sc, Li and Sr are well balanced and are mostly accounted by clinopyroxene, which contains more than 80% of LREE and Sr, 60–70% of Li and Sc. Orthopyroxene contributes to the Sc and Li, budget whereas olivine is most significant for the Li budget. Most of the LREE and Li
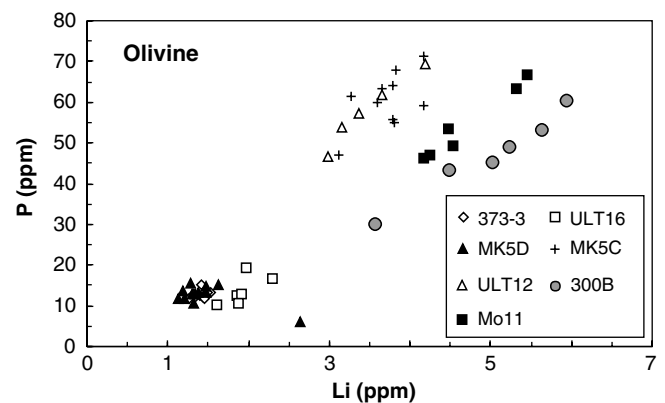
Fig. 11 P–Li in olivine and of the analysed sample set

bulk-rock budgets are therefore hosted by the spinel-facies minerals. On the other hand, most LILE (U, Pb, Rb, see Fig. 12) are unbalanced because the measured bulk rock contents in this sample are much higher than the calculated ones. This likely implies that LILE are hosted in retrograde (not analysed) phases formed during minor aqueous fluid influx. In the case of Ba, nearly 90% of this element is incorporated into retrograde amphibole, which has a modal abundance of only half a
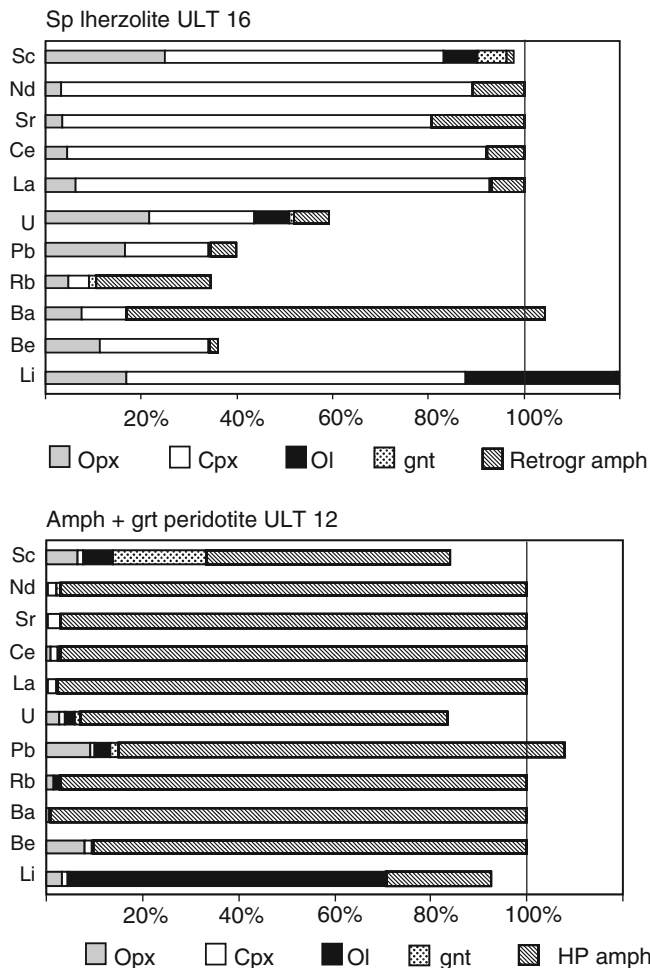
Sp lherzolite ULT 16

Amph + grt peridotite ULT 12

Fig. 12 Trace element distribution among the rock-forming minerals in the spinel lherzolite ULT16 and in the garnet + amphibole peridotite ULT12. The following modal abundances of minerals were obtained based on petrographic and from mass balance by Rampone and Morten (2001). ULT16: orthopyroxene 27%, clinopyroxene 14%, olivine 57%, garnet 1%, retrograde amphibole 0.5%. Nd, Sr, Ce, La exceeded 120% and have been recalculated to 100. ULT12: orthopyroxene 19%, clinopyroxene 1%, olivine 57%, garnet 3%, high-pressure amphibole 20%. La, Sr, Ce, Nd, Rb, Ba exceeded 120% and have been recalculated to 100

percent. Also, retrograde serpentine veins might accommodate some LILE.

The mass balance thus demonstrates that enrichment in LREE and Li must have occurred under spinel-facies conditions (1,200°C, ~1.5 GPa). Nevertheless, the LILE patterns of the bulk rock do not fully represent an enrichment at spinel-facies conditions, as the LILE whole-rock budgets are strongly affected by minor amounts of retrograde phases. For this reason, in the forthcoming discussion we will use the LILE abundances measured in the single mineral phases, rather than the bulk-rock compositions, to discuss the metasomatic imprint of the spinel facies lherzolites.

In the garnet–amphibole peridotite most trace elements appear balanced (Fig. 12). Amphibole hosts nearly all LILE and LREE. Garnet, although present only in small amounts, contributes to the Sc (and HREE) budget. The main host of Li is olivine. The key trace elements visible in bulk-rock patterns are all hosted in phases that are stable in the garnet + amphibole peridotite facies and hence retrograde processes do not seem to have a significant effect. Therefore, the characteristic enrichment of LILE and LREE in these samples is related to metasomatic processes that occurred during fluid influx in the high pressure-low temperature equilibration in the garnet + amphibole stability field (850°C; 3.0 GPa).

The trace element compositions of the Ulten peridotites: comparable metasomatic signatures by different agents

Previous studies of the Ulten peridotites agree on the fact that the transformation of hot litospheric spinel-peridotites (T = 1,200°C; P = 1.5 GPa) into amphibole ± garnet peridotites occurred during a temperature decrease to 850°C, pressure increase to 3 GPa and influx of an aqueous subduction fluid. Nimis and Morten (2000) related such an evolution to corner flow in the mantle wedge, causing lateral motion followed by tectonic slicing into the subducting plate. The infiltration of subduction fluids in the cooled wedge peridotites is documented by the stability of amphibole with garnet (Fig. 2b) and by the occurrence of coexisting phlogopite and amphibole in sample 300B. Moreover, the LREE- and incompatible element-enriched fingerprint of the amphibole ± garnet peridotites (Figs. 8, 9) is clear evidence of aqueous fluid influx in these systems at the transition from dry spinel lherzolites to wet garnet + amphibole peridotites. The associated crustal rocks were identified as the possible fluid sources (Rampone and Morten 2001). The trace element dataset presented here confirms the above features and further documents significant enrichment of bulk rocks and of single minerals in incompatible elements, particularly LILE, LREE and Li. Based on the estimates of Nimis and Morten (2000), such a fluid-induced recrystallization in the garnet-facies fits a subduction zone geotherm: Fig. 13 emphasizes that this stage took place in the subsolidus field for a hydrous peridotite system, and above the wet solidus for granitic and pelitic systems (Hermann 2003).

We have shown that the LREE- and Li-enriched signature also pertains to the starting lithospheric spinel-lherzolites unaffected by the garnet-facies recrystallization (Fig. 2a). This signature is held by the spinel-facies pyroxenes, which pre-date garnet and which display disequilibrium features with it, as emphasized by the high HREE contents of pyroxenes in the spinel lherzolites. The temperature at this initial stage was above the wet peridotite solidus (Fig. 13). As a consequence, metasomatism of the spinel lherzolites cannot be explained by the addition of an aqueous fluid because: (1) no pargasitic spinel-facies amphibole is present in these rocks; (2) fluid infiltration at 1,200°C would have caused peridotite partial melting and incompatible element loss

from the peridotite residue. Therefore, the criptic metasomatism of the spinel lherzolites can be related to melt percolation at high temperature.

Based on the petrologic frame and on the crystallization temperatures (Fig. 13) we thus conclude that the metasomatic imprints affecting the spinel- and the garnet + amphibole peridotites were driven by infiltration of two different agents: a melt (high-temperature metasomatism) and a fluid phase (lower-temperature metasomatism), respectively. In the following we discuss the most striking features of the Ulten peridotite varieties, trying to emphasize possible geochemical keys to distinguish the effects of melt versus fluid as the agent leading to the mantle metasomatism.

Spinel lherzolites

One main result of our work is that all analysed samples, spinel- and amphibole ± garnet peridotites, share a comparable metasomatic imprint, as all bulk rocks and major rock-forming minerals display enrichments in LREE relative to HFSE. The spinel-peridotites depleted in major elements (e.g. ULT16), display concave bulk REE patterns enriched in LREE (Fig. 3). The mineral phases responsible for this signature are the coarse, spinel-facies, orthopyroxene and clinopyroxene (Figs. 5, 6, 12). The LREE-enriched patterns of the spinel lherzolites are likely related to chromatographic effects of porous melt flow at distance from the melt source (Bodinier et al. 1990). This mechanism creates LREE

Fig. 13 *P*–*T* diagram reporting the thermobarometric estimates of the spinel and of the garnet + amphibole peridotites. The wet solidus for granitic, pelitic and wet peridotite systems are also reported. See the text for explanation

fractionation and variable degrees of LREE enrichment regardless of the type of metasomatic agent. The spinel-facies pyroxenes also display positive spikes in Pb, U, Li, detectable Cs and Ba and relative depletion in Nb, Ta, Zr, Hf. LILE enrichment with respect to HFSE is generally taken as evidence for a subduction-related signature in mantle rocks and in magmas. On the other hand, as discussed by Ionov et al. (2002), negative HFSE anomalies can also be related to chromatographic fractionation during porous melt flow (as a result of amphibole precipitation near the melt source), without reflecting an initial melt signature. However, the significant enrichment in Pb, U, Li of clinopyroxene from the Ulten spinel lherzolites, together with the petrologic evidence of high-temperature metasomatism, strongly suggests interaction with a subduction-related melt (Ionov et al. 2002; Churikova et al. 2001). It is notheworthy that clinopyroxene does not record the concomitant increase in other LILE (e.g. Be, Rb, K). Regarding Be, the available experimental data indicate that $^{cpx/melt}D_{Be}$ is very low (0.002–0.1), up to ten times lower than $^{cpx/melt}D_{Li}$ (0.1–0.2) (Brenan et al. 1998), and this could explain the observed Li/Be fractionation, with normalized Li higher than normalized Be (Figs. 5, 6), in the spinel-facies clinopyroxenes.

The Li variability in olivine, clinopyroxene and orthopyroxene also suggests interaction with a mafic melt during this early spinel-facies criptic metasomatism. Li behaves as moderately incompatible during peridotite partial melting. Seitz and Woodland (2000) defined a Li-depletion trend in coexisting olivine and pyroxenes in a set of equilibrated spinel and garnet peridotites and observed constancy in the inter-mineral partitioning of Li. This trend is represented by the coarse shaded line in Fig. 14. According to Seitz and Woodland (2000) partial melting shifts the peridotite minerals to lower Li contents along the grey line of Fig. 14, whereas the equilibrium re-enrichment has the opposite effect. Deviation from this behaviour is documented for several metasomatized peridotites showing preferential Li enrichment either in olivine or in pyroxene, depending on the dominant type of metasomatism. Interaction with mafic melts generally produces Li-enriched pyroxenes (Seitz and Woodland 2000; see the black arrow in Fig. 14). The average Li contents of the Ulten spinel-facies olivine and pyroxenes are plotted in Fig. 14a, b. Clinopyroxene and orthopyroxene are enriched in Li and display a disequilibrium Li partitioning with olivine consistent with an exchange with a percolating, presumably mafic, melt. It is remarkable that in the spinel lherzolites clinopyroxene is the mineral containing the highest amounts of Li: $^{cpx/opx}D_{Li}$ ranges from 3 in sample 373 to 7 in ULT 16; $^{cpx/ol}D_{Li}$ are 2.7 and 8, respectively. Clinopyroxene is thus the main host of Li although it makes only 15% of the modal abundance.

In summary, thermobarometry, phase relations and the metasomatic style of the spinel lherzolites indicate that they were part of a mantle wedge layer fluxed by melts rising from a deeper source of subduction-related magmas and carrying recycled crustal components.
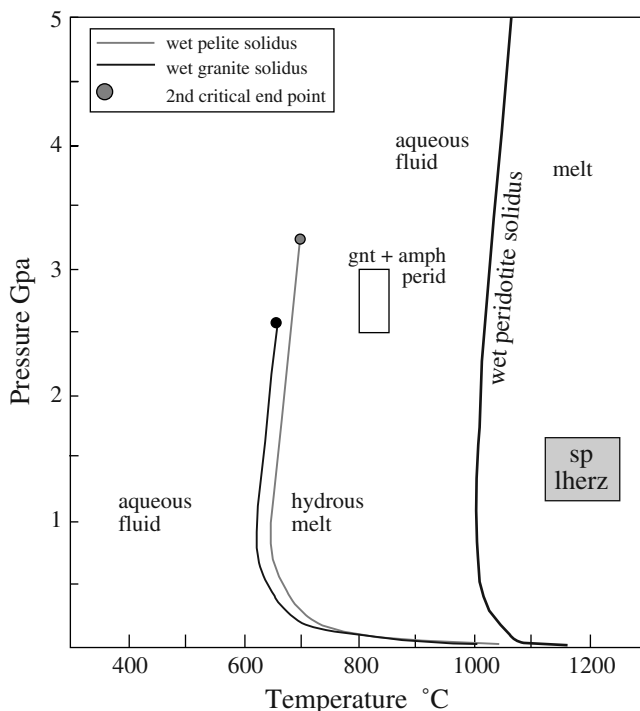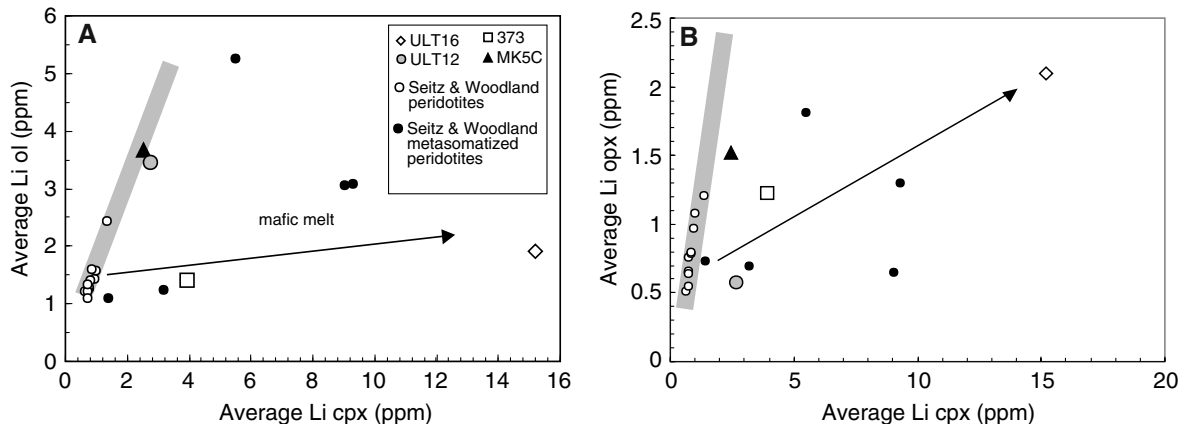
Fig. 14 a, b Li variability in olivine, orthopyroxene and clinopyroxenes from the spinel and from the amphibole + garnet peridotite samples. The Li-depletion trends in equilibrated peridotites (*grey lines*) and the literature data of Seitz and Woodland (2000) are reported for comparison

Amphibole + garnet peridotites

Among the amphibole + garnet peridotites, our study individuates ULT12 as best representative of the eclogite-facies hydration, since this sample still preserves garnet and clinopyroxene in textural and chemical equilibrium with amphibole, olivine and orthopyroxene. In ULT12 amphibole shows HREE-depleted compositions indicating full equilibrium with garnet and clinopyroxene (Fig. 9). Relevant features of the trace element composition of ULT12 (and the other garnet peridotite MK5C) are the bulk-rock positive anomalies in Cs, Ba, Pb and U reported in Fig. 3c. Bulk Li and Be in these two samples are twice the PM. The LILE and LREE enriched signature is nearly entirely hosted in amphibole and clearly reflects addition of a crustal component to the mantle rocks. As shown in Fig. 4 the coupled increase of water (represented by the modal contents of amphibole), Sr and Pb, together with positive Pb–Sr and Pb–U correlations, further indicate that the incompatible element increase in these samples is fluid-mediated.

A distinctive feature of the amphibole + garnet peridotites is the strong LILE/HFSE fractionation outlined by the elevated bulk-rock and mineral (e.g. amphibole and pyroxenes) contents in several LILE and by relatively low Nb, Ta, Zr and Hf. Pb_N/Nb_N in garnet-facies clinopyroxenes is 300–600, i.e. much higher than in the precursor spinel lherzolites (16–90). Another relevant difference concerns the low Ce/Pb values of pyroxenes in the garnet + amphibole peridotites (1.4–2.7 in clinopyroxene) compared with the spinel-facies pyroxenes (2.6–25 in clinopyroxene). This is strong evidence that Pb was added to the garnet peridotites by an infiltrating subduction fluid and further suggests an involvement of different metasomatic agents during the evolution of the Ulten peridotites.

In the garnet-facies samples, the olivine–clinopyroxene pairs display much different Li contents compared with the spinel peridotites (Fig. 14), thus reflecting different within-mineral partitioning behaviour. In the

garnet + amphibole peridotites, amphibole and olivine approach the Li concentrations of clinopyroxene and the partitioning approaches unity with $^{cpx/amph}D_{Li} = 0.7$–0.8 and $^{cpx/ol}D_{Li} = 0.7$–0.8, in samples MK5C and ULT 12. In the garnet + amphibole samples, therefore, clinopyroxene/olivine partitioning of Li changes drastically, being up to ten times lower than in the spinel-facies rocks. In these samples olivine is thus able to incorporate appreciable amounts of Li, and because of its high modal abundance, olivine becomes the principle host of Li. The increased capability of olivine grown in the presence of a fluid phase to incorporate Li is also emphasized in Fig. 11, showing that olivine in the garnet + amphibole and amphibole peridotites contains much higher Li and P than olivine from the anhydrous spinel lherzolite precursors. Mantle olivine equilibrated with a fluid phase thus appears an important Li repository: this confirms previous studies showing that olivine interacting with a slab agent (Tomascak et al. 2002) and/or coexisting with a dehydration fluid (e.g. the antigorite breakdown fluid; Scambelluri et al. 2004), uptake significant amounts of Li due to favourable olivine-fluid partitioning. Another remarkable geochemical feature in the Ulten peridotites concerns the distribution of Li and Be in clinopyroxene. The spinel-facies clinopyroxene (ULT16 and 373) has higher normalized Li than Be; on the other hand, the garnet-facies one (ULT12 and MK5C) displays the opposite trend, with higher normalized Be than Li. This might be explained with the available experimental data on clinopyroxene/melt/fluid partitioning (Brenan et al. 1998), indicating that Be in clinopyroxene is more compatible than Li in the presence of an aqueous fluid, whereas the opposite behaviours is observed in the presence of a melt phase.

Amphibole-peridotites

The comparison of garnet + amphibole peridotites with amphibole peridotites MO11 and 300B (lacking

clinopyroxene and garnet and dominated by HREE-enriched amphiboles as the result of garnet breakdown) does not show significant changes in the trace element variability. Besides the HREE enrichment, the amphibole stable with garnet and the one overgrowing garnet display the same characteristic patterns in LILE and LREE. This likely implies that fluids fluxing the Ulten peridotites at these stages are continuously sourced from the same crustal rock types. Phlogopite, found in the amphibole peridotite 300B, provides further evidence of LILE-enriched aqueous fluid metasomatism. Olivine is not often used to monitor metasomatic processes because of its overall low trace element content. However, P and Li in olivine (Fig. 11), track the entire metasomatic history of the Ulten peridotite suite. The transition from spinel to amphibole ± garnet peridotites is accompanied by an abrupt coupled increase of P and Li contents of olivine. Within the amphibole ± garnet peridotites, Li increases from the amphibole + garnet samples ULT12 and MK5C, to the amphibole-peridotites MO11 and 300B. We suggest that the Li and P contents of olivine are a useful geochemical tool to investigate mantle metasomatism.

Implications for dynamics of the Ulten wedge peridotites

The features discussed above enable to distinguish between melt- and fluid-mediated metasomatism in the Ulten peridotites and present clues to track the pathway of mantle wedge domains from lithospheric regions percolated by uprising melts to deeper and cooler levels

fluxed by subduction fluids (Fig. 15). The starting spinel-peridotites are located in a relatively hot domain above an asthenospheric melt source, their signature strongly suggests that the percolating melt was produced in a mantle region enriched in some crustal components. The significant Pb, U and Li enrichment that characterizes the metasomatic fingerprint is a distinctive feature of subduction-related zone magmas and can be achieved through the exchange with such a melt type. Our dataset thus fits a slab-to-mantle transfer of elements as expected in supra-subduction wedges and the overall process recorded by the early spinel peridotites might be reasonably related with the Variscan subduction of continental crust (Fig. 15). However, due to the lack of age constraints for this pristine spinel-facies metasomatism, we cannot exclude that this signature was achieved during an older (pre-Variscan?) episode of continental subduction which caused the re-enrichment of this lithospheric mantle domain (Petrini and Morten 1993).

Lateral corner-flow motion brings the spinel-peridotite towards the subducting slab and into a P–T regime where fluids are likely released from the slab (Scambelluri and Philippot 2001; Manning 2004). Our data agrees with previous studies, proposing that this fluid must derive from subducted crustal material in the vicinity of the peridotites. The exact mechanism of this metasomatism is still mysterious. According to previous models, transformation into amphibole ± garnet peridotites occurred once the spinel-facies rocks were tectonically sliced inside the subducting slab (Nimis and Morten 2000; Rampone and Morten, 2001). Sm–Nd dating of the peridotites, country migmatites and
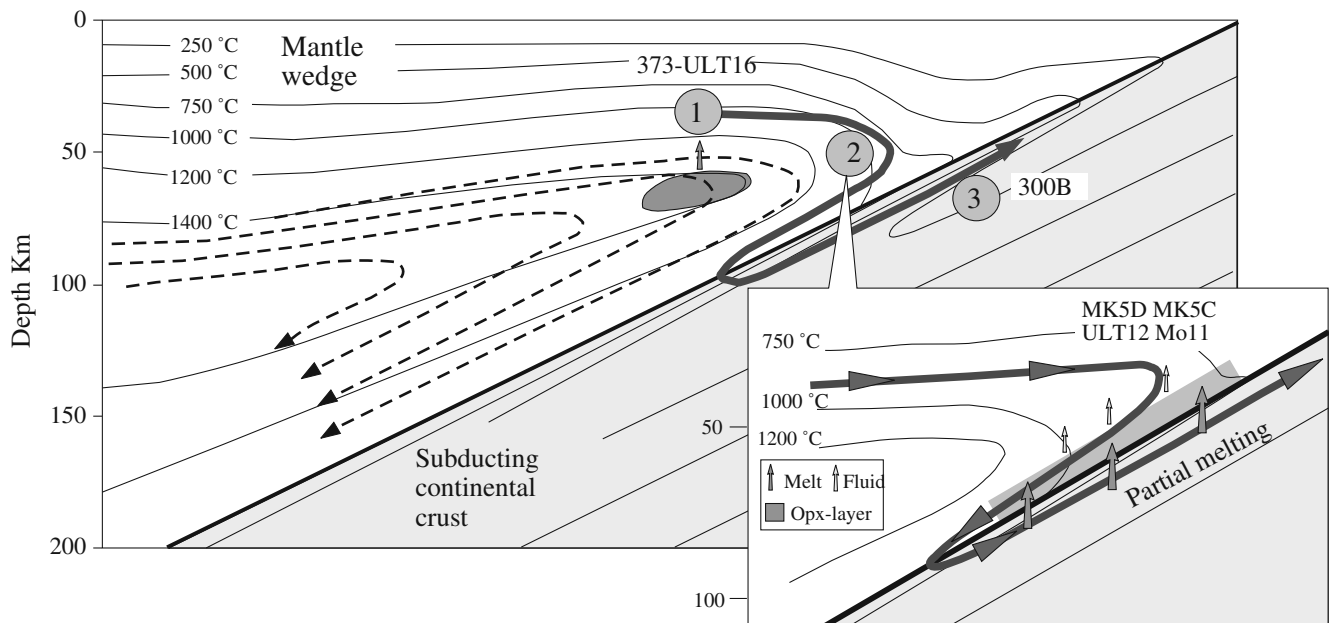

Fig. 15 General scenario for the Ulten peridotite evolution (after Nimis and Morten 2000). Infiltration of melts (*stage 1*) in the spinel facies field, is followed by peridotite hydration in a wedge setting above the subducting crust (*stage 2* and *inset*), entrainment in the slab and exhumation (*stage 3*). See text for explanation

eclogites yield late Variscan garnet–whole rock and garnet–clinopyroxene ages of about 330 Ma, indicating that tectonic incorporation of peridotites into the slab and partial melting of the crustal rocks took place at eclogite-facies conditions (Tumiati et al. 2003). However, the metasomatic style of the amphibole + garnet peridotites indicates that the main agent was an aqueous fluid, not a siliceous melt, and lack of diffuse orthopyroxene overgrowths in these rocks is compelling evidence that siliceous melt infiltration was not the dominant process. This led Rampone and Morten (2001) to propose that leucosome crystallization liberated residual aqueous fluids responsible for metasomatism in the associated garnet peridotites. Although this could be a viable mechanism to precipitate silicates and liberate a free water-rich fluid, some main uncertainties remain. The peridotite slices inside the slab are volumetrically subordinated to the surrounding migmatites: melts should have infiltrated and interacted with the peridotite slices, but this is not observed in terms of extensive orthopyroxene, garnet and phlogopite precipitation. Moreover, the liberation of an aqueous fluid due to leucosome crystallization is difficult to achieve as long as the slab temperature is above the wet pelite solidus. As an alternative scenario, we envisage here the possibility that fluid infiltration occurred when the garnet peridotites still were sited in the mantle wedge above the subducting crust (Fig. 15). The hydrous partial melts uprising from the slab interacted with the overlying peridotites precipitating their Si overload to produce an orthopyroxene-rich layer. This layer could have acted as a filter for the slab agents, enhancing precipitation of the most compatible elements and leaving a residual aqueous fluid enriched in the most incompatible ones (e.g. LILE, LREE, light elements). An analogous filtering mechanism has been proposed for the formation of metasomatic orthopyroxene and of multiphase solid microinclusions in garnet orthopyroxenites from Dabie-Shan (Malaspina et al. 2005). Upward migration of the residual aqueous fluid and its interaction with the mantle wedge led to formation of the amphibole + garnet peridotites, which were subsequently entrained in the slab. This mechanism enhances large-scale production of aqueous fluids enriched in incompatible elements starting from hydrous melts released by crustal slab components under high (and ultrahigh) pressure conditions. In such a scenario, the incorporation of the peridotites into the country rock gneisses might have occurred during exhumation and not during peak metamorphism, in contrast to earlier models on the formation of these peridotite lenses within crustal rocks.

Conclusions

In the Ulten Zone, transformation of coarse spinel peridotites into amphibole ± garnet peridotites occurred as the result of corner-flow movements inside a mantle wedge above a subducting continental slab during the Variscan orogeny. Our major result is that a full sample set representative of the entire wedge history shares a comparable geochemical signature, featuring the enrichment in LREE, LILE and light elements with respect to HFSE. These characteristics imply the recycling of crustal-derived components in various wedge domains. Based on the significantly different recrystallization temperatures recorded by the metasomatized sample suite (1,200°C in the dry spinel peridotites; 850°C in the amphibole + garnet peridotites) we propose that melt and fluid agents were responsible for the metasomatic imprint of the spinel and of the garnet + amphibole peridotites, respectively.

We attribute the criptic metasomatism of spinel lherzolites (Pb, U, Li and LREE-enrichment) to a percolating mafic melt. Li-enrichment of the spinel-facies pyroxenes (up to 24 ppm Li) and $^{cpx/opx}D_{Li} = 3-7$ together with $^{cpx/ol}D_{Li} = 2.7-8$ point to clinopyroxene as major Li sink at this stage. The style of enrichment suggests that the percolating melt was subduction-related.

The garnet + amphibole peridotites re-crystallized at eclogite-facies conditions in presence of an aqueous fluid. These peridotites are enriched in Cs, Ba, Pb, U, Sr Li, LREE; coupled with amphibole (±phlogopite) crystallization clearly reflect the fluid-mediated addition of crustal components to mantle wedge domains above the subducting slab. $^{cpx/amph}D_{Li} = 0.7$ and $^{cpx/ol}D_{Li} = 0.7-0.8$ indicate that olivine becomes the principal Li hosts in the garnet samples. Such a marked change in clinopyroxene–olivine Li partitioning with respect to the spinel lherzolites, indicates that olivine grown in the presence of fluid behaves as a sink for Li. The subduction fluid at this stage was sourced by crustal rocks which were undergoing partial melting with production of hydrous granitic liquids. We suggest that reaction of these hydrous melts with the overlying wedge peridotites led to Si and Al precipitation into an orthopyroxene-rich layer. This filtering process likely produced the LILE-enriched residual fluid which infiltrated the wedge peridotites to form the garnet + amphibole metasomatized peridotites.

Successive retrograde re-equilibration during garnet + amphibole peridotite ascent towards the surface is accompanied by minor changes (e.g. increase of HREE and Li in amphibole, increase of Li and decrease of P in olivine) which do not affect the trace element signature acquired at eclogite-facies. Along their entire history, the Ulten wedge peridotites were percolated first by melts and then by fluids adding recycled components likely sourced from a similar crustal reservoir.

References

Andersen T, Neumann ER (2001) Fluid inclusions in mantle xenoliths. Lithos 55:301–320

Bebout GL, Barton DM (1993) Metasomatism during subduction: products and possible paths in the Catalina Schist, California. Chem Geol 108:61–92

Benciolini N, Poli S (1993) The lower continental crust in the Tonale Nappe (Upper Austroaline, Ultental): new petrological constraints. Terra Nova 5(1):98

Bodinier JL, Vasseur G, Vernieres J, Dupuy C, Fabries J (1990) Mechanisms of mantle metasomatism: geochemical evidence from the Lherz orogenic peridotite. J Petrol 31:597–628

Brenan JM, Shaw HF, Ryerson FJ, Phinney DL (1995) Mineral–aqueous fluid partitioning of trace elements at 9008°C and 2.0 GPa: constraints on the trace element chemistry of mantle and deep crustal fluids. Geochim Cosmochim Acta 59:3331–3350

Brenan JM, Ryerson FJ, Shaw HF (1998) The role of aqueous fluids in the slab-to-mantle transfer of boron, beryllium and lithium during subduction: experiments and models. Geochim Cosmochim Acta 62:3337–3347

Brueckner HK (1998) Sinking intrusion model for the emplacement of garnet-bearing peridotites into continent collision orogens. Geology 26(7):631–634

Churikova T, Dorendorf F, Wörner G (2001) Sources and fluids in the mantle wedge below Kamchatka, evidence from across-arc geochemical variation. J Petrol 42:1567–1593

Domanik KJ, Hervig RL, Peacock SM (1993) Beryllium and boron in subduction zone minerals: an ion microprobe study. Geochim Cosmochim Acta 57:4997–5010

Elliott T, Jeffcoate A, Bouman C (2004) The terrestrial Li isotope cycle: light-weight constraints on mantle convection. Earth Planet Sci Lett 220:231–245

Godard G, Martin S, Prosser G, Kienast JR, Morten L (1996) Variscan migmatites, eclogites and garnet-peridotites of the Ulten zone, Eastern Austroalpine system. Tectonophysics 259:313–341

Hermann J (2003) Experimental evidence for diamond-facies metamorphism in the Dora-Maira massif. Lithos 70:163–182

Hoinkes G, Thoeni M (1993) Evolution of the O E tztal-Stubai, Scarl-Campo and Ulten basement units. In: von Raumer J, Neubauer F (eds) The pre-Mesozoic geology in the Alps. Springer, Berlin Heidelberg New York, pp 485–494

Ionov D, Bodinier JL, Mukasa SB, Zanetti A (2002) Mechanisms and sources of mantle metasomatism: major and trace element compositions of Peridotite Xenoliths from Spitsbergen in the context of numerical modelling. J Petrol 43:2219–2259

van Keken P (2003) The structure and dynamics of the mantle wedge. Earth Planet Sci Lett 215:323–338

Kessel R, Schmidt MW, Ulmer P, Pettke T (2005) Trace element signature of subduction-zone fluids, melts and supercritical liquids at 120–180 km depth. Nature 437:724–727

Laurora A, Mazzucchelli M, Rivalenti G, Vannucci R, Zanetti A, Barbieri MA, Cingolani CA 2001 Metasomatism and melting in carbonated peridotite xenoliths from the mantle wedge: the Gobernador Gregores case (Southern Patagonia). J Petrol 42:69–87

Leeman WP (1996) Boron and other fluid-mobile elements in volcanic arc lavas: implications for subduction processes. In: Bebout GE, Sholl DW, Kirby SH, Platt JP (eds) Sub-duction: top to bottom, geophysical monograph, AGU, vol 96, pp 269–276

Malaspina N, Hermann J, Scambelluri M, Compagnoni R (2005) Trace element transfer in the mantle wedge: evidence from polyphase inclusions in garnet pyroxenites (Dabie-Shan, China). In: Proceedings of the 7th international eclogite conference, Mitt. Osterr. Miner. Ges., 150, 100

Manning CE (2004) The chemistry of subduction-zone fluids. Earth Planet Sci Lett 223:1–16

Martin H, Smithies RH, Rapp R, Moyen JF, Champion D (2005) An overview of adakite, tonalite-trondhjemite-granodiorite (TTG), and sanukitoid: relationships and some implications for crustal evolution. Lithos 79:1–24

Maury RC, Defant MJ, Joron JL (1992) Metasomatism of the sub-arc mantle inferred from trace-elements in philippine xenoliths. Nature 360:661–663

McDonough WF, Sun SS (1995) The composition of the Earth. Chem Geol 120:223–253

Moran AE, Sisson VB, Leeman WP (1992) Boron depletion during progressive metamorphism: implications for subduction processes. Earth Planet Sci Lett 111:331–349

Morten L, Obata M (1983) Possible high-temperature origin of pyroxenite lenses within garnet peridotite, Northern Italy. Bull Mineral 106:775–780

Morten L, Obata M (1990) Rare earth abundances in the eastern Alpine peridotites, Nonsberg area Northern Italy. Eur J Mineral 2:643–653

Nimis P, Morten L (2000) P ± T evolution of 'crustal' garnet peridotites and included pyroxenites from Nonsberg area (upper Austroalpine), NE Italy: from the wedge to the slab. J Geodyn 30:93–115

Obata M, Morten L (1987) Transformation of spinel lherzolite to garnet lherzolite in ultramac lenses of the austridic crystalline complex, Northern Italy. J Petrol 28:599–623

Paquin J, Altherr R (2002) Subduction-related lithium metasomatism during exhumation of the Alpe Arami ultrahigh-pressure garnet peridotite (Central Alps, Switzerland). Contrib Mineral Petrol 143:623–640

Paquin J, Altherr R, Ludwig T (2004) Li–Be–B systematics in the ultrahigh-pressure garnet peridotite from Alpe Arami (Central Swiss Alps): implications for slab-to-mantle wedge transfer. Earth Planet Sci Lett 218:507–519

Pearce NJG, Perkins WT, Westgate JA, Gorton MJ, Jackson SE, Neal CR, Chenery SP (1997) A compilation of new and published major and trace element data for NIST SRM 610 and NIST SRM 612 glass reference materials. Geostand Newsl 21:115–144

Petrini R, Morten L (1993) Nd-isotopic evidence of enriched lithospheric domains: an example from the Nonsberg area, eastern Alps. Terra Abstr 4:19–20

Rampone E, Morten L (2001) Records of crustal metasomatism in the garnet peridotites of the Ulten Zone (Upper Austroalpine, Eastern Alps). J Petrol 42:207–219

Scambelluri M, Philippot P (2001) Deep fluids in subduction zones. Lithos 55:213–227

Scambelluri M, Müntener O, Ottolini L, Pettke T, Vannucci R (2004) The fate of B, Cl and Li in the subducted oceanic mantle and in the antigorite breakdown fluids. Earth Planet Sci Lett 222:217–234

Schiano P, Clocchiatti R, Shimizu N, Maury RC, Jochum KP, Hofmann AW (1995) Hydrous, silica-rich melts in the subarc mantle and their relationships with erupted arc lavas. Nature 377:595–600

Seitz HM, Woodland AB (2000) The distribution of lithium in peridotitic and pyroxenitic mantle lithologies—an indicator of magmatic and metasomatic processes. Chem Geol 166:47–64

Szabo C, Bodnar RJ, Sobolev AV (1996) Metasomatism associated with subduction-related, volatile-rich silicate melt in the upper mantle beneath the Nograd-Gomor volcanic field, northern Hungary southern Slovakia: evidence from silicate melt inclusions. Eur J Mineral 8:881–899

Tatsumi Y (1989) Migration of fluid phases and genesis of basalt magmas in subduction zones. J Geophys Res 94:4697–4707

Tenthorey E, Hermann J (2004) Composition of fluids during serpentinite breakdown in subduction zones: evidence for limited boron mobility. Geology 32:865–868

Tomascak PB, Widom E, Benton LC, Goldstein SL, Ryan JC (2002) The control of lithium budgets in island arcs. Earth Planet Sci Lett 196:227–238

Trial AF, Rudnick RL, Ashwal LD, Henry DJ, Bergman SC (1984) Fluid inclusions in mantle xenoliths from Ichinomegata, Japan (Abstr.). EOS 65, p 306

Tumiati S, Thoeni M, Martin S, Nimis P, Mair V (2003) Mantle–crust interactions during Variscan subduction in the Eastern Alps (Nonsberg–Ulten zone): geochronology and new petrological constraints. Earth Planet Sci Lett 210:509–526

Van Roermund HLM, Carswell AD, Drury M, Heijborer TC (2002) Microdiamonds in a megacrystic garnet websterite pod from Bardane on the island of Fjortoft, western Norway: evidence for diamond formation in mantle rocks during deep continental subduction. Geology 30:959–962

Vidal P, Dupuy C, Maury R, Richard M (1989) Mantle metasomatism above subduction zones—trace-element and radiogenic isotope characteristics of peridotite xenoliths from Batan Island (Philippines). Geology 17:1115–1118

Wilson SA (1997) The collection, preparation, and testing of USGS reference material BCR-2, Columbia River, Basalt, U.S. Geol. Surv. Open-File Report 98

Woodland AB, Seitz HM, Altherr R, Marschall H, Olker B, Ludwig T (2002) Li abundances in eclogite minerals: a clue to a crustal or mantle origin? Contrib Mineral Petrol 143:587–601

Workman RK, Hart SR (2005) Major and trace element composition of the depleted MORB mantle (DMM). Earth Planet Sci Lett 231:53–72

Zack T, Tomascak PB, Rudnick RL, Dalpe C, McDonough WF (2003) Extremely light Li in orogenic eclogites: the role of isotope fractionation during dehydration in subducting oceanic crust. Earth Planet Sci Lett 208:279–290

Zheng JP, Zhang RY, Griffin WL, Liou JG, O'Reilly SY (2005) Heterogeneous and metasomatized mantle recorded by trace elements in minerals of the Donghai garnet peridotites, Sulu UHP terrane, China. Chem Geol 221:243–259